HHS Public Access

Author manuscript

Sci Signal. Author manuscript; available in PMC 2023 February 19.

Published in final edited form as:

Sci Signal. 2022 October 25; 15(757): eabn9009. doi:10.1126/scisignal.abn9009.

Yap and Taz promote osteogenesis and prevent chondrogenesis in neural crest cells in vitro and in vivo

Xiaolei Zhao[1], **Li Tang**[2], **Tram P. Le**[1], **Bao H. Nguyen**[3], **Wen Chen**[1], **Mingjie Zheng**[1], **Hiroyuki Yamaguchi**[1], **Brian Dawson**[4], **Shuangjie You**[1,5], **Idaliz M. Martinez-Traverso**[3], **Shannon Erhardt**[1,5], **Jianxin Wang**[2], **Min Li**[2], **James F. Martin**[3,6], **Brendan H. Lee**[4], **Yoshihiro Komatsu**[1,5], **Jun Wang**[1,5,*]

[1]Department of Pediatrics, McGovern Medical School, The University of Texas Health Science Center at Houston, Houston, Texas 77030, USA

[2]Hunan Provincial Key Lab on Bioinformatics, School of Computer Science and Engineering, Central South University, Changsha, Hunan 410083, China

[3]Department of Molecular Physiology and Biophysics, Baylor College of Medicine, One Baylor Plaza, Houston, Texas 77030, US

[4]Department of Molecular and Human Genetics, Baylor College of Medicine, One Baylor Plaza, Houston, Texas 77030, USA

[5]MD Anderson Cancer Center and UT Health Graduate School of Biomedical Sciences, The University of Texas, Houston, Texas 77030, USA

[6]Texas Heart Institute, Houston, Texas 77030, USA

Abstract

Neural crest cells (NCCs) are multipotent stem cells that can differentiate into multiple cell types, including the osteoblasts and chondrocytes, and constitute the majority of the craniofacial skeleton. Here, we show through in vitro and in vivo studies that the transcriptional regulators Yap and Taz have redundant functions as key determinants of the specification and differentiation of NCCs into osteoblasts or chondrocytes. Primary and cultured NCCs deficient in *Yap* and *Taz* switched from osteogenesis to chondrogenesis, and NCC-specific deficiency for *Yap* and *Taz* resulted in bone loss and ectopic cartilage in mice. Yap bound to the regulatory elements of key genes that govern osteogenesis and chondrogenesis in NCCs and directly regulated the expression

*Corresponding author. jun.wang@uth.tmc.edu.

Author Contributions

X.Z. and Jun Wang designed the research study. X.Z., L.T., T.P.L., B.H.N, W.C., M.Z., H.Y., B.D., I.M.M.-T., S.E., and Jun Wang performed the research. X.Z., L.T., S.Y., Jianxin Wang, M.L., Y.K., and Jun Wang analyzed the data. J.F.M. and B.H.L. provided reagents. X.Z., L.T., Y.K., and Jun Wang wrote the manuscript.

Competing Interests

The authors declare that they have no competing interests.

Data and Materials availability

The CUT&RUN and CUT&Tag datasets have been deposited to the National Center for Biotechnology Information Gene Expression Omnibus under the accession number of GSE154332. All other data are present in the main manuscript or the Supplementary Materials. Study materials will be available upon reasonable request under material transfer agreements with The University of Texas Health Science Center at Houston. Further information and requests for resources and reagents should be directed to and will be fulfilled by the Lead Contact, Jun Wang (jun.wang@uth.tmc.edu).

of these genes, some of which also contained binding sites for the TCF/LEF transcription factors that interact with the Wnt effector β-catenin. During differentiation of NCCs in vitro and NCC-derived osteogenesis in vivo, Yap and Taz promoted the expression of osteogenic genes such as *Runx2* and *Sp7* but repressed the expression of chondrogenic genes such as *Sox9* and *Col2a1*. Furthermore, Yap and Taz interacted with β-catenin in NCCs to coordinately promote osteoblast differentiation and repress chondrogenesis. Together, our data indicate that Yap and Taz promote osteogenesis in NCCs and prevent chondrogenesis, partly through interactions with the Wnt–β-catenin pathway.

INTRODUCTION

Neural crest cells (NCCs), which have been described as “the fourth germ layer,” can differentiate into several different cell types such as osteoblasts, chondrocytes, smooth muscle cells, neurons, and other cell types to generate a wide variety of derivatives during vertebrate embryogenesis. This makes NCCs a unique stem cell population and an ideal model system to study the molecular signals that regulate cell fate decisions in stem and progenitor cells (1, 2). The majority of craniofacial bone originates from NCCs (3, 4). The NCC-derived ecto-mesenchymal stem cells (eMSCs) that give rise to craniofacial bone differ from the perivascular mesenchymal stem cells (MSCs) that contribute to long bone. There are two different types of ossification: endochondral and intramembranous. Endochondral ossification proceeds through a cartilage intermediate wherein MSC-derived chondrocytes deposit cartilage matrix and then undergo cell death, after which the cartilage matrix is replaced with bone by MSC-derived osteoblasts. In contrast, intramembranous ossification is performed by eMSCs that differentiate into osteoblasts that form bone without a cartilage intermediate. Long bone is formed through endochondral ossification, whereas most craniofacial bone is formed through intramembranous ossification (3, 4). Despite long-standing interest and progress in understanding the gene regulatory networks involved in NCC-derived craniofacial skeleton formation (5, 6), the molecular signals that guide cell fate decisions and differentiation in NCCs and determine whether NCC-derived eMSCs become osteoblasts that produce craniofacial bone or chondrocytes that produce cartilage are not well understood.

Hippo-Yap signaling is a fundamental pathway that regulates organ size and plays pivotal roles in development and various diseases (7, 8). The Hippo signaling pathway is composed of a cascade of kinases. In the absence of repression by Hippo signaling, the downstream effectors Yap and Taz function as transcriptional co-activators that promote gene expression in the nucleus by partnering with transcription factors such as TEA domain (TEAD) family members. Upon the phosphorylation of Yap and Taz by Hippo signaling, they are excluded from the nucleus, thereby becoming transcriptionally inactive. Yap and Taz activity can also be modulated by Hippo-independent factors such as the tyrosine kinase focal adhesion kinase (FAK) (9), the serine-threonine kinase nemo-like kinase (NLK) (10), the cell adhesion protein αE-catenin (11, 12), and transcriptional coactivator vestigial like family member 4 (VGLL4) (13). Yap and Taz play important roles in regulating the stemness and differentiation of normal embryonic and adult stem cells, as well as cancer stem cells (14-18). In the process of osteogenesis and long bone formation by

bone marrow–derived MSCs (bmMSCs), Yap and Taz have been shown to play critical yet controversial roles. In murine bmMSCs and embryonic-derived MSCs, Taz interacts with the transcription factor Runx2 to promote osteogenesis and repress adipogenesis (15, 19). Consistent with this, the double knockdown of *YAP* and *TAZ* in human bmMSCs has been shown to repress osteogenesis while activating adipogenesis (20). In mice, *Yap* deletion in the osteoblast lineage using the *Ocn-Cre* driver increases adipocyte formation and reduces osteoblast differentiation, resulting in trabecular bone loss (21), and deleting both *Yap* and *Taz* in osteoblasts using the *Osterix-Cre* driver impairs long bone accrual and remodeling (22). In contrast, *YAP1* overexpression in human bmMSCs blocks both osteogenesis and adipogenesis (23). In the context of chondrogenesis, Yap and Taz, especially Yap, have been shown to function as negative regulators of chondrogenesis in both murine and human MSCs (24-26). However, Yap has also been reported to promote early chondrocyte proliferation and inhibit late chondrocyte maturation in mice (27). On the other hand, Taz promotes both chondroprogenitor proliferation and chondrocyte maturation in mice, and *Taz* expression gradually increased during chondrogenic differentiation (28). In another study, Yap and Taz activity enhanced chondrocyte proliferation in vitro but was dispensable for chondrocyte proliferation in vivo (29). Despite the emerging roles of Yap and Taz in osteogenesis and chondrogenesis in embryonic and bone marrow–derived stem cells, it is unclear whether they play similar roles in NCC-derived eMSCs and the craniofacial skeleton, which is composed of intramembranous bone and nonmineralized cartilage.

Studies have indicated that the Hippo-Yap pathway has a critical role in NCCs and NCC-derived tissues (30-32). In familial studies, *YAP1* mutations were found to be associated with orofacial clefting and intellectual disability (33). Impaired HIPPO-YAP signaling has also been reported to be associated with human anencephaly (34). In avian embryos, Yap and TEAD promote the migration of NCCs (31, 35), and, in mice, the deletion of *Yap* and *Taz* specifically in NCCs causes early embryonic lethality at embryonic day (E) 10.5, which is before skeleton morphogenesis (36). Here, we show evidence that Yap and Taz have a pivotal role in orchestrating NCC-derived cell fate determination toward osteoblasts versus chondrocytes and provide insight into the molecular regulation underlying this process.

RESULTS

Yap and Taz are required for osteoblast differentiation and inhibit chondrogenesis in NCCs in vitro

O9-1 NCCs are multipotent cells originally isolated from E8.5 mouse embryos and can differentiate into osteoblasts, chondrocytes, glia, or smooth muscle cells under defined culture conditions (37, 38). To study the effect of changes in Yap and Taz activity on NCC osteoblast differentiation, we cultured O9-1 NCCs in osteoblast differentiation medium and performed knockdown (KD) studies using an siRNA smart pool targeting both *Yap* and *Taz* (siY/T) or a scrambled siRNA (siCtrl). *Yap* and *Taz* expression were significantly decreased in *Yap* and *Taz* double KD (*Yap*/*Taz* dKD) cells compared with control cells (fig. S1A). Cells were harvested at multiple time points (Fig. 1A). Under culture conditions for osteogenic differentiation, O9-1 NCCs showed gradually decreasing amounts of the stemness marker Sox2, which has been implicated in maintaining the pluripotency of stem

cells (39), and increased accumulation of the osteoblast markers alkaline phosphatase (ALP) and specificity protein-7 (SpP7, also called osterix) over time (Fig. 1B). These data, taken together with previous findings (37, 38), indicated that O9-1 NCCs are an efficient in vitro model in which to study NCC-derived osteoblast differentiation.

After culturing O9-1 NCCs in osteoblast differentiation medium for 10 days, we evaluated osteoblast differentiation by performing Alizarin red staining, which labels mineralized extracellular matrix deposited by differentiated osteoblasts and calcium deposits in osteocytes. We found that Alizarin red–stained control cells had large amounts of extracellular calcium deposits, whereas *Yap*/*Taz* dKD cells had significantly less extracellular matrix mineralization (Fig. 1C and fig. S1B). Notably, *Yap*/*Taz* dKD cells displayed morphology different from that of the control cells and resembled chondrocytes rather than osteoblasts (arrow, Fig. 1C). To confirm this finding, we performed Alcian blue staining, which labels cartilage. The *Yap*/*Taz* dKD cells with chondrocyte-like morphology indeed stained positive for Alcian blue (Fig. 1D and fig. S1C).

Immunofluorescence staining further indicated that control cells robustly produced the osteoblast marker osteocalcin (Ocn), whereas few *Yap*/*Taz* dKD cells were Ocn^+ (Fig. 1E). However, the accumulation of the chondrocyte marker Col2a1 was significantly greater in *Yap/Taz* dKD cells compared with control cells (Fig. 1F). In concordance with these observations, we found that, compared with control cells, *Yap*/*Taz* dKD cells showed significantly increased abundance of the chondrogenic marker Sox9 and decreased abundance of the osteogenic marker Runx2 (Fig. 1G). Using Western blot analysis, we also evaluated osteogenic and chondrogenic markers at different time points during differentiation (Fig. 1, H-J). After cells were cultured in osteoblast differentiation medium for 2 days (d2), Sox9, which is required for the initiation of chondrogenesis, was significantly increased in *Yap*/*Taz* dKD cells compared with control cells (Fig. 1H). The chondrocyte marker Col2a1 was minimally present at d2, but it was significantly more abundant in *Yap*/*Taz* dKD cells than in control cells at both d5 (Fig. 1I) and d10 (Fig. 1J). In contrast, *Yap/Taz* dKD cells showed opposite trends in osteogenic markers. Although no obvious change was observed at d2 (Fig. 1H), the abundance of Runx2, which is required for the initiation of osteogenesis, was significantly lower in *Yap/Taz* dKD cells than in control cells after 5 and 10 days of culture (Fig. 1, I and J). Furthermore, the osteoblast differentiation marker Sp7 was significantly decreased in *Yap/Taz* dKD cells compared with control cells at d10 (Fig. 1J). Overall, Western blot data indicated a trend of an increased chondrogenic signature and decreased osteogenic signature in *Yap*/*Taz* dKD cells compared with control cells. These data indicate that Yap and Taz are required for osteogenesis in NCCs and that their deficiency results in a switch to chondrogenesis.

Yap knockout arrests differentiating NCCs as osteochondral precursors in vitro

We previously used CRISPR/Cas9-mediated genome editing to efficiently generate *Yap* knockout (KO) O9-1 NCCs, which have the same region of *Yap* deletion as the mouse *Yap* conditional KO allele (36). When these *Yap* KO cells were cultured in osteoblast differentiation medium for 10 days, Alizarin red staining showed that, similar to *Yap*/*Taz* dKD cells, they failed to form mature osteoblasts with mineralized extracellular matrix

compared with wild-type (WT) cells (Fig. 2A and fig. S1D). However, *Yap* KO cells did not show the chondrocyte morphology (Fig. 2A) that *Yap*/*Taz* dKD cells did (Fig. 1C). In accordance with these observations, *Yap* KD cells also did not stain positive for Alcian blue (Fig. 2B and fig. S1E). In addition, immunofluorescence staining showed that, unlike WT cells that robustly produced the osteoblast marker Ocn, few *Yap* KO cells were Ocn^{+} (Fig.2C). However, few *Yap* KO cells were positive for the chondrocyte differentiation marker Col2a1 (Fig. 2D). Whereas *Yap*/*Taz* dKD promoted the differentiation of NCCs into chondrocytes instead of osteoblasts, *Yap* KO prevented the proper differentiation of NCCs into either cell type.

We further found that, compared with control cells, *Yap* KO cells had increased amounts of both the early osteogenic marker Runx2 and the chondrogenic marker Sox9 (Fig. 2E). Moreover, the percentage of cells that were positive for both Runx2 and Sox9, characterized as osteochondral progenitors, was significantly increased in *Yap* KO cells compared with WT cells (Fig. 2E). These data suggested that *Yap* KO cells were arrested at the osteochondral progenitor stage, which was further corroborated by Western blotting for osteogenic and chondrogenic markers and by the observation that the abundance of the stemness marker Sox2 was significantly increased in *Yap* KO cells compared with WT cells at all stages of differentiation (Fig. 2, F-H). At d5 and d10, amounts of both the osteoblast marker Sp7 and the chondrocyte marker Col2a1 were decreased in *Yap* KO cells compared with WT cells (Fig. 2, G and H). These data indicated that *Yap* KO cells differentiated into neither osteoblasts nor chondrocytes, most likely due to arresting at the osteochondral progenitor stage characterized by the presence of Runx2, Sox9, and Sox2. Throughout the differentiation process, Taz was significantly increased in *Yap* KO cells compared with WT cells (Fig. 2, F-H), suggesting that it played a compensatory role that was sufficient to prevent a cell fate switch to chondrogenesis during osteoblast differentiation but was not sufficient to support the differentiation of either cell type.

To address whether the arrest of *Yap* KO cells at the osteochondral precursor stage depended on the compensatory increase in Taz, we knocked down *Taz* in *Yap* KO cells (*Yap* KO *Taz* KD, fig. S1F) and cultured the cells under osteoblast differentiation conditions. Instead of undergoing osteoblast differentiation like control cells (Fig. 2I), a majority of the *Yap* KO *Taz* KD NCCs differentiated into chondrocytes, as indicated by the production of Col2a1 (Fig. 2J), which recapitulated the phenotypes seen in *Yap/Taz* dKD NCCs (Fig. 1, E and F). These data further indicated that Yap and Taz play critical yet functionally redundant roles in the NCC cell fate decision and differentiation into osteoblasts versus chondrocytes.

Yap and *Taz* deficiency results in defective NCC-derived cranial bone formation in mice

Cranial NCCs are capable of differentiating into either osteoblasts or chondrocytes and contribute to the majority of craniofacial skeleton during embryo development (40). To study the functions of Yap and Taz in NCCs in vivo, we used the NC-specific Cre drivers *Wnt1-Cre* and *Wnt1-Cre2* to generate conditional knockout (CKO) mice lacking *Taz* and *Yap* specifically in NCCs, but focused on $Wnt1\text{-}Cre2^{Tg/+}$ to avoid the previously reported ectopic Wnt1 activity of *Wnt1-Cre* (41). Previously, we showed that $Yap^{-/-}$;$Taz^{-/-}$ double CKO (Yap/Taz dCKO) and *Yap* single KO caused embryonic lethality at E10.5 and severe

phenotypes such as vascular defects (36). We also found that CKO embryos homozygous for the floxed *Taz* allele and heterozygous for the floxed Yap allele (*Yap*$^{+/-}$;*Taz*$^{-/-}$), which lack *Taz* and retain only a single copy of *Yap*, showed no obvious defects at E10.5 (36). Here, we found that compared with control mice, *Yap*$^{+/-}$;*Taz*$^{-/-}$ CKO mutants exhibited calvaria bone defects with varying amounts of severity from E14.5 to the postnatal period , including nasal, frontal, and interparietal bones (Fig. 3A-C and fig. S2A-G).

These cranial bone defects were consistently observed at different embryonic and postnatal stages. For instance, unlike 2-week-old controls that had well-formed frontal and interparietal bones, 2-week-old *Yap*$^{+/-}$;*Taz*$^{-/-}$ CKO mutants had visibly defective frontal and interparietal bones (fig. S2A). Compared with control littermates, 3-week-old *Yap*$^{+/-}$;*Taz*$^{-/-}$ CKO mutants had visibly defective nasal and interparietal bones (fig. S2B). *Yap*$^{+/-}$;*Taz*$^{-/-}$ CKO mutants showed reduced bone density in the nasal and frontal bones (fig. S2C) and in the interparietal bones (fig. S2D) compared with control mice, as seen in radiographs. Furthermore, compared with control mice, *Yap*$^{+/-}$;*Taz*$^{-/-}$ CKO mutants had defective bone mineralization in the nasal and frontal bones (Fig. 3A) and in the interparietal bones (Fig. 3B), as seen on micro-computed tomography (μCT) scans.

Whole-mount Alizarin red and Alcian blue staining revealed disturbed NCC-derived cranial bone formation with defective mineralization at different stages. Compared with E18.5 littermate control mice, *Yap*$^{+/-}$;*Taz*$^{-/-}$ CKO mutants showed visibly missing bone mineralization in NCC-derived cranial bones, including nasal, frontal, and interparietal bones (Fig. 3C), whereas non–NCC-derived parietal bone formation was not affected. In concordance with these observations, *Yap*$^{+/-}$;*Taz*$^{-/-}$ CKO mutants also showed defects in NCC-derived bone at postnatal day 1 (P1, fig. S2F) and P5 compared to littermate controls (fig. S2G). Together, these findings revealed that Yap and Taz have indispensable roles in the development of NCC-derived cranial bones.

Yap and Taz play redundant roles in NCCs in vivo

Some *Yap*$^{+/-}$;*Taz*$^{+/-}$ double heterozygous mice showed mild defects in NCC-derived bones. Alizarin red and Alcian blue staining indicated that, unlike control littermates, *Yap*$^{+/-}$;*Taz*$^{+/-}$ double heterozygotes had Wormian bones, which are extra bones that occur within sutures of the skull, in the frontal bone region at P5 but no obvious defects in the interparietal bone region (fig. S2H). Consistent with these findings, μCT analysis of 3-week-old *Yap*$^{+/-}$;*Taz*$^{+/-}$ heterozygous mice also showed no apparent defects in the interparietal bone region (fig. S2I) but Wormian bone formation in the frontal bone region that was not observed in controls (fig. S2J). Von Kossa staining showed that, compared with controls, E18.5 *Yap*$^{+/-}$;*Taz*$^{+/-}$ heterozygous mice showed mild defects in bone mineralization (fig. S2K). Safranin O staining indicated the presence of ectopic chondrocytes in the anterior frontal suture region of E18.5 *Yap*$^{+/-}$;*Taz*$^{+/-}$ heterozygous mice but not in that of control littermates (fig. S2L). These data indicate that, during NCC-derived cranial skull cap formation, Yap and Taz have redundant functions in cell fate determination and differentiation of NCCs into osteoblasts versus chondrocytes.

Yap and Taz deficiency reduces osteoblast differentiation and increases chondrocyte differentiation in vivo and ex vivo

To further analyze the NCC-derived cranial bone defects caused by simultaneous loss of Taz and reduction of Yap, we first evaluated cell proliferation in *Yap*$^{+/-}$;*Taz*$^{-/-}$ CKO mutants and control littermates. 5-ethynyl-2'-deoxyuridine (EdU) staining revealed no obvious differences in cell proliferation between *Yap*$^{+/-}$;*Taz*$^{-/-}$ CKO mutants and control littermates (fig. S2M). Next, we examined osteoblast and chondrocyte differentiation and bone mineralization in NCC-derived craniofacial regions. *Yap*$^{+/-}$;*Taz*$^{-/-}$ CKO mutants showed disrupted osteoblast differentiation and ectopic cartilage formation, which was consistent with our in vitro observations. Compared with control embryos, E18.5 *Yap*$^{+/-}$;*Taz*$^{-/-}$ CKO mutants displayed defective ossification and mineralization in the frontal bone (Fig. 3D) and interparietal bone (fig. S2E), as indicated by Von Kossa staining. Immunofluorescence staining further indicated that, compared with controls, Sp7^{+} cells, indicating osteoblasts, were significantly decreased in the developing frontal bone region of *Yap*$^{+/-}$;*Taz*$^{-/-}$ CKO mutants (Fig. 3E).

In agreement with our in vitro data, we observed ectopic cartilage formation in NCC-derived regions of *Yap*$^{+/-}$;*Taz*$^{-/-}$ CKO mutants at different stages, as indicated by Safranin O staining. For example, compared with controls, all E18.5 *Yap*$^{+/-}$;*Taz*$^{-/-}$ CKO mutants showed ectopic cartilage in the NCC-derived frontal suture region of coronal sections (Fig. 3F). Unlike controls, in which no ectopic cartilage was detected, 2-week-old *Yap*$^{+/-}$;*Taz*$^{-/-}$ CKO mutants also showed ectopic cartilage in the interparietal bone regions of sagittal sections (Fig. 3, G and H). Additionally, compared with control littermates, these mutant mice exhibited abnormal structures of the lambdoid suture due to aberrant interparietal bone development and damaged trabecular bone (Fig. 3G). Together, these data indicated that *Yap* and *Taz* deficiency led to reduced osteoblast differentiation and ectopic cartilage formation in vivo.

Because *Yap*$^{+/-}$;*Taz*$^{-/-}$ CKO mutants have one normal copy of *Yap* that may support some normal Yap and Taz functions in NCC-derived osteochondral differentiation phenotype in vivo, we performed ex vivo experiments in which we knocked down *Yap* and *Taz* in cells isolated from embryos. MSCs from the NCC-derived frontal portion of E13.5 *Wnt1-Cre2*$^{Tg/+}$;*mTmG*$^{-/-}$ mouse embryos, which express GFP in NCCs, were isolated and cultured in osteoblast differentiation medium with *siY/T* and *siCtrl* treatment. We used this transgenic reporter mouse line (42), which expresses green fluorescent protein (GFP) in the presence of Cre, to track the NCC lineage (Fig. 3I). Compared with control cells, *Yap/Taz* dKD cells showed significantly reduced amounts of *Yap* and *Taz* transcripts (Fig. 3J). Consistent with our in vitro and in vivo results, 21 days after culture in osteoblast differentiation medium, isolated NCC-derived MSCs with *Yap/Taz* dKD showed a substantial decrease in mineralized extracellular matrix compared with control cells (Fig. 3K). *Yap/Taz* dKD cells, but not control cells, formed chondrocytes (Fig. 3L). These data indicated that *Taz* and *Yap* deficiency impaired osteoblast differentiation and promoted aberrant chondrocyte formation ex vivo.

Yap regulates the expression of osteogenic and chondrogenic genes and Wnt target genes in NCCs

Our in vitro, ex vivo, and in vivo findings indicated that Yap and Taz play a critical role in determining whether NCCs undergo osteogenesis versus chondrogenesis. To further examine their roles during this process and to identify downstream target genes on a genomic scale, we performed CUT&RUN-seq (cleavage under targets and release using nuclease sequencing) and CUT&Tag-seq (cleavage under targets and tagmentation sequencing) in O9-1 NCCs using antibodies against Yap1, H3K27me3, and IgG. Because CUT&RUN and CUT&Tag are similar experiments that yielded similar results, the CUT&RUN-seq data are used as representative here. Both the CUT&RUN-seq and CUT&Tag-seq datasets have been deposited to the National Center for Biotechnology Information Gene Expression Omnibus under accession number GSE154332. We further analyzed the CUT&RUN-seq data in combination with ATAC-seq (assay for transposase-accessible chromatin with high-throughput sequencing) data from human NCCs (accession no. GSE70751) (43) and cranial NCC-derived tissues in E10.5 mouse embryos (accession no. GSE89436) (44). Yap binding was enriched in active open chromatin regions indicated by ATAC-seq data instead of inactive chromatin regions indicated by H3K27me3 CUT&RUN-seq (Fig. 4A). When we further examined the genomic regions occupied by Yap, we found that about 19% of Yap was bound to promoter regions, 44% to intergenic regions, and 33% to intronic regions (Fig. 4B). Gene ontology (GO) term analysis revealed that, among the top-enriched GO terms, Yap-bound genes are involved in ossification, osteoblast differentiation, and chondrocyte differentiation (Fig. 4C), which further supports Yap's key role in NCC-derived osteogenesis versus chondrogenesis.

To obtain additional information about which target genes were activated by Yap (decreased expression in *Yap*/*Taz* dCKO mutants) or repressed by Yap (increased expression in *Yap/Taz* dCKO mutants), we overlapped the putative Yap target genes identified by CUT&RUN-seq with differentially expressed genes identified in RNA sequencing (RNA-seq) data from the E10.5 mandibular tissues of *Yap/Taz* dCKO mutants and control embryos (GSE69311) (Fig. 4D). The top GO terms suggested that Yap target genes regulate different cell events and processes (Fig. 4, E and F). Of note, after *Yap* and *Taz* deletion, we observed increased expression of Yap target genes encoding products that in turn regulate the intrinsic apoptotic signaling pathway, programmed cell death, and cell maturation (Fig. 4, E and G). On the other hand, the expression of Yap target genes encoding products that regulate growth, stem cell population maintenance, and ossification were decreased (Fig. 4, F and G). The top-enriched GO terms for transcripts that were decreased after *Yap* and *Taz* deletion were significantly associated with canonical Wnt signaling (Fig. 4, F and G), suggesting a potential positive interaction between *Yap* and *Taz* and the canonical Wnt signaling pathway.

Motif analysis implicates coordinated gene regulation by Yap, Taz, and β-catenin in NCCs

Motif analysis of our Yap CUT&RUN-seq data and the published ATAC-seq data from human NCCs (GSE70751) (43) revealed that TEAD and TCF/LEF motifs were highly represented in the top motifs associated with both YAP and open chromatin in NCCs (Fig. 5A). Transcription factors of the TCF/LEF family are major mediators of the Wnt signaling by binding with transcriptional coactivator β-catenin, the key effector of canonical Wnt

signaling. At a genomic scale, TEAD and TCF/LEF motifs have similar peak localizations and region-gene associations in both O9-1 NCCs (Fig. 5, B-D) and human NCCs (fig. S3, A-C). A genome-wide analysis showed that 38.9% (1904 out of 4898) of genes that are potentially regulated by Yap/Taz and are enriched in TEAD motifs are also enriched in TCF/LEF motifs within the same open chromatin regions (Fig. 5E), suggesting the direct and coordinated regulation of these genes by Yap/Taz-TEAD and β-catenin–TCF/LEF complexes. GO term analysis of these genes indicated that many are important regulators of skeletal system development, ossification, extracellular matrix, cartilage development, and cell growth (fig. S3D).

The key osteogenic gene *Runx2* (Fig. 5F) and the key chondrogenic genes *Sox9* (Fig. 5G) and *Sox5* (fig. S3E) contain multiple overlapping TEAD and TCF/LEF motifs in the active regions of chromatin in O9-1 NCCs identified by CUT&RUN-seq data and mouse ATAC-seq data. This suggests that these genes are potentially coregulated by Yap/Taz and β-catenin. *Runx2*, *Sox9*, and *Sox5* also contain multiple TEAD and TCF/LEF motifs that overlap in the active regions of chromatin in human NCCs (fig. S3, F-I). In addition, TEAD and TCF/LEF binding motifs colocalize in human neural crest disease–associated enhancers (EC1.25, EC1.45) of *Sox9* (fig. S3I), which drive the Pierre Robin sequence (PRS), a congenital birth defect characterized by craniofacial abnormalities such as micrognathia and cleft palate (45). Together, these data suggest that Yap/Taz and β-catenin may coordinate to regulate target gene expression in NCCs at a genomic scale.

Yap interacts with β-catenin in NCCs

To determine whether Yap interacts with β-catenin in NCCs, we performed coimmunoprecipitation studies in O9-1 NCCs. We performed immunoblotting for Yap and β-catenin in Yap and nonspecific immunoglobulin G (IgG) immunoprecipitates. The signal for β-catenin was strong in control cells but markedly decreased in *Yap*/*Taz* dKD cells, and the signal for β-catenin was undetectable when using IgG as the immunoprecipitation antibody in control cells, indicating that Yap and β-catenin are present in the same complex in O9-1 NCCs (Fig. 6A). When we used the proximity ligation assay (PLA) to further evaluate the interaction and location of Yap and β-catenin in NCCs, Yap strongly interacted with β-catenin in control cells, as indicated by the detection of PLA signal (red spots) in both cytoplasm and nuclei (Fig. 6B). In contrast, in *Yap/Taz* dKD cells, the interaction between Yap and β-catenin was significantly decreased in nuclei (Fig. 6B). PLA signaling also indicated that the interaction between Yap and β-catenin in nuclei substantially increased during the differentiation of NCCs into osteoblasts (Fig. 6B), suggesting the possibility that this interaction promotes NCC differentiation. Consistent with this finding, β-catenin was enriched in the nuclei of control NCCs after 2 days of differentiation, and the colocalization of Yap and β-catenin was higher in the nuclei of control cells than in those of *Yap*/*Taz* dKD cells (Fig. 6C). These data suggested that Yap interacts with β-catenin to promote the differentiation of NCCs into osteoblasts.

Yap, Taz, and β-catenin promote osteogenesis in vitro by cooperatively preventing chondrocyte differentiation

To gain additional insight into whether Yap, Taz, and β-catenin cooperate in orchestrating NCC osteogenesis versus chondrogenesis, we performed *Yap*, *Taz,* and *β-catenin* single KDs*, Yap/Taz* dKD, and *Yap/Taz/β-catenin* triple KD (tKD) in O9-1 NCCs and evaluated osteogenic and chondrogenic gene expression at time points after culturing the cells in osteoblast differentiation medium. The chondrogenic marker Sox9 was increased in all KD cells at both d2 and d5 compared with control cells (Fig. 6, D and E, and fig. S4B). The *Yap/Taz/β-catenin* tKD cells had the greatest increase in Sox9 among all the KD cells at both d2 and d5 (Fig. 6 D and E, and Fig. S4B) and significantly increased Sox9 compared with *Yap/Taz* dKD cells at d5 (fig. S4B, and Fig. 6E). These findings suggested that Yap, Taz, and β-catenin function together to inhibit *Sox9* expression. In contrast, the osteogenic marker Runx2 was significantly reduced in *Yap/Taz/β-catenin* tKD cells compared with control cells at d2 (Fig. 6D and fig. S4A) and d5 (fig. S4B). However, in *Yap/Taz* dKD cells, Runx2 was remarkably decreased at d5 compared with control cells (fig. S4B) and was not significantly different at d2 compared with control cells (Fig. 6D and fig. S4A). The changes in Runx2 abundance in different groups were milder than the changes in Sox9. This further supported that Yap, Taz, and β-catenin function together to promote osteogenesis and prevent cell fate switching to chondrocytes.

We next evaluated the chondrocyte marker Col2a1 and osteoblast marker Col1a1 at d5. Col1a1 was significantly decreased in all types of KD cells compared with control cells and was the lowest in *Yap/Taz/β-catenin* tKD cells among all conditions (Fig. 6F). However, Colla1 was not significantly different between *Yap/Taz/β-catenin* tKD and *Yap/Taz* dKD cells (Fig. 6F). In contrast, Col2a1, encoded by gene that is a known direct transcriptional target of Sox9, was significantly increased in all types of KD cells, except *Yap* KD cells, compared with control cells (Fig. 6F). Notably, the *Yap/Taz/β-catenin* tKD cells had the most significantly increased abundance of Col2a1 among all KD cells. Col2a1 was significantly higher in *Yap/Taz/β-catenin* tKD cells than in *Yap/Taz* dKD cells (Fig. 6F). Together, these findings further indicated that Yap, Taz, and β-catenin promote osteogenesis in NCCs by coordinately preventing chondrogenesis.

Yap and Taz regulate osteogenic and chondrogenic genes in vivo

We evaluated the expression of osteogenic and chondrogenic potential Yap candidate target genes in response to *Yap* and *Taz* deficiency ($Yap^{+/-};Taz^{-/-}$) in vivo. As shown in the sagittal view of an E18.5 control mouse embryo, $Runx2^{+}$ cells, which tend to differentiate into osteoblasts, were found in the frontal bone (Fig. 7A, and fig. S5A), whereas $Sox9^{+}$ cells, which tend to differentiate into chondrocytes, were found in the same location of E18.5 $Yap^{+/-};Taz^{-/-}$ CKO mutant embryos (Fig. 7B, and fig. S5B), suggesting a cell fate switch from osteoblasts to chondrocytes. To label NCCs in vivo, we generated $Yap^{+/-};Taz^{-/-}$ CKO mutants in a genetic background that included the mTmG reporter, which expresses GFP in a Cre-dependent manner. In *Wnt1-Cre2*; $Yap^{+/-}$;$Taz^{-/-}$;$mTmG^{+/-}$ mice, the Cre driver induces GFP expression and *Yap* and *Taz* knockout in NCCs. As shown in coronal views of E18.5 embryos, NCC-derived cells expressed GFP (Fig. 7, C and D). In $Yap^{+/-}$;$Taz^{-/-}$ CKO mutants, most $Sox9^{+}$ cells were GFP^{+}, indicating that they were NCC-derived cells (Fig.

7D). Sox9^{+} cells were found in the ectopically formed cartilage regions of *Yap*$^{+/-}$;*Taz*$^{-/-}$ CKO mutants but not in the corresponding regions of controls (Fig. 7C).

Sox5 and Sox6 are known to cooperate with Sox9 to promote chondrogenesis (46). The Sox9^{+} cells found in the ectopic cartilage of E18.5 *Yap*$^{+/-}$;*Taz*$^{-/-}$ CKO mutants were also positive for Sox6, whereas NCC-derived cells in the same location of controls were positive for Runx2 but not Sox6 (Fig. 7, E and F). Similarly, Sox5 and Col2a1 were found in the Sox9^{+} cells of the ectopic cartilage of E18.5 *Yap*$^{+/-}$;*Taz*$^{-/-}$ mutant mice but were not found in the same location in controls (Fig. 7, G and H). Of note, in E18.5 *Yap*$^{+/-}$;*Taz*$^{+/-}$ heterozygous mice, cells in the metopic suture region with ectopically formed cartilage were also positive for Sox9 (fig. S5D), Sox6 (fig. S5F), Sox5, and Col2a1 (Fig. S5H), although not to the extent observed in *Yap*$^{+/-}$;*Taz*$^{-/-}$ CKO mutants. In contrast, cells in the corresponding regions of the littermate controls produced Runx2 (figs. S5E) but not Sox9 (fig. S5C), Sox6 (fig. S5E), Sox5, or Col2a1 (fig. S5G). Together, these data further indicated that Yap and Taz favor osteogenesis and repress chondrogenesis in NCCs.

DISCUSSION

As multipotent stem cells, NCCs make extensive contributions to vertebrate embryogenesis. How they make cell fate decisions, however, remains a fundamental biological question (2). In this study, we revealed that Yap and Taz promote osteogenesis in NCCs by preventing chondrogenesis in vitro, ex vivo, and in vivo during NCC-derived skull cap development, partially through cooperation with β-catenin (Fig. 8). These data provide important insights into NCC fate determination and differentiation.

The majority of the craniofacial skeleton and MSCs in sutures are derived from NCCs (47-50). Here, we showed that Yap and Taz likely play a key role in NCC-derived osteogenic versus chondrogenic cell fate determination and differentiation, which can be a potential mechanism to ensure that the skull bones undergo intramembranous ossification rather than endochondral ossification during NCC-derived skull development. *Yap* and *Taz* dKD in O9-1 cells and primary NCC-derived eMSCs, as well as *Yap*$^{+/-}$;*Taz*$^{-/-}$CKO in mice caused defective NCC-derived osteoblast differentiation and, notably, a possible cell fate switch from osteogenesis to chondrogenesis. These findings in NCCs are distinct from those in bmMSCs, in which deficiency for Yap and Taz promotes a fate switch from osteogenesis to adipogenesis without any obvious alteration of chondrogenesis (21), suggesting that Yap and Taz play different roles in cell fate determination and differentiation in different stem cell types. In addition, Yap and Taz were reported to function differently at various stages during bmMSC osteogenesis. *Yap* and *Taz* deletion in osteoprogenitors promotes osteoblast differentiation, whereas their deletion in mature osteoblasts and osteocytes resulted in decreased osteoblast number and bone formation (51). Our data suggests that the roles of Yap and Taz in NCC-derived osteogenesis are also probably stage-dependent. We found that Yap and Taz most likely maintained the multipotent status of NCCs to prevent NCC-derived eMSC differentiation. However, after eMSCs were specified as osteochondral progenitors, Yap and Taz promoted an osteoblast versus chondrocyte cell fate, and *Yap* and *Taz* deficiency caused NCC-derived osteochondral progenitors to differentiate into chondrocytes instead of osteoblasts. Unlike the more robust switch into chondrocytes due

to *Yap and Taz* double deficiency in vitro, thus far, these changes were only observed in the skull cap in the $Yap^{+/-}$;$Taz^{-/-}$ CKO mutants instead of throughout NCC-derived skull structures. An important limitation of our in vivo model is that the mutant embryos retain a single functional copy of *Yap*, which may be sufficient to support some of the redundant roles of Yap and Taz in vivo or in a subset of skull structures. Also, NCC-derived eMSC osteogenesis in vivo is more complex that of NCCs in vitro and regulated by an intricate signaling network (52). We also cannot exclude the possibility that *Yap* and *Taz* only function in a certain group of NCC-derived eMSCs instead of all NCCs, which is worthy further investigations in future.

Yap and *Taz* have been shown to play overlapping or sometimes different—or even contrasting—roles in different contexts. Furthermore, their divergent roles depend on multiple factors such as cell type and time window (53, 54). Here, we found that *Yap* and *Taz* have overlapping roles during NCC-derived osteogenesis. Distinct from the severe frontal and interparietal bone damage with ectopic cartilage formation that occurred in $Yap^{+/-}$;$Taz^{-/-}$ mutants, $Yap^{+/-}$;$Taz^{+/-}$ double heterozygous mice showed mild NCC-derived bone formation defects, including ectopic cartilage and Wormian bone formation, suggesting a functional overlapping between *Yap* and *Taz* in NCCs. $Yap^{+/-}$;$Taz^{-/-}$ CKO mutants showed defective osteogenesis and ectopic cartilage formation only in the skull cap instead of all NCC-derived skull structures, perhaps because one function copy of *Yap* is sufficient to support normal formation of the other skull structures. Taz also has an essential role in preventing NCC-derived osteochondral progenitors from undergoing chondrogenesis, given that *Yap* deletion in NCCs led to the compensatory high expression of *Taz* and arrested osteochondral status, whereas the additional KD of *Taz* led to chondrocyte formation. The overlapping function of Yap and Taz in NCCs may also explain why not all cells underwent chondrogenesis in the *Yap*/*Taz* dKD experiments and why chondrogenesis was not more widespread in $Yap^{+/-}$;$Taz^{-/-}$ CKO mutants.

In this study, we found that Yap and Taz directly regulated key genes that affect the osteochondral lineage cell fate decision and differentiation, and that loss *Yap* and *Taz* led to changes in the in vivo and in vitro expression of these key genes, which included but were not limited to the key osteogenesis gene *Runx2* and key chondrogenesis genes *Sox9* and *Sox5*, both of which have conserved TEAD-binding motifs. The cell fate commitment of MSCs to the osteoblastic lineage requires the key transcription factor Runx2, whereas the cell fate commitment to the chondrogenic lineage is controlled by Sox family transcription factors Sox9, Sox5, and Sox6. Sox9 is the key factor to initiate chondrogenesis in osteochondral progenitor cells and functions through the cooperation of Sox5 and Sox6 (46, 55-58). Inactivation of *Sox9* in NCCs leads to loss of chondrogenic potential, resulting in the complete absence of cartilages and endochondral bones derived from cranial NCCs in mice (59). Studies also showed that patients with cleidocranial dysplasia (CCD) who had *RUNX2* mutations also had failed closure of anterior and posterior fontanelles (60). In addition, the CKO of *Runx2* in NCCs in mice led to defective ossification in certain regions of craniofacial bone, primarily in the anterior half of the craniofacial bones, including nasal and frontal bones. Furthermore, mouse embryos with the heterozygous loss of *Runx2* showed impaired closure of the frontal bone at the metopic suture (61). These findings are in line with our in vivo findings in *Yap* and *Taz*–deficient mouse embryos.

Yap and Taz are known transcriptional coactivators. Here, we found that they function as transcriptional coactivators of osteogenic genes and corepressors of chondrogenic genes in NCCs, partially through their interaction with β-catenin, which is a key downstream transcriptional coactivator of canonical Wnt signaling. The canonical Wnt signaling pathway plays a critical role in regulating NC induction, migration, and differentiation, and β-catenin is a key factor in stem cell fate determination and differentiation. In bmMSCs, Runx2 is directly activated by β-catenin to initiate osteogenesis (62). The lack of β-catenin results in the high expression of *Sox9, Sox5*, and *Sox6*, leading to the commitment of bmMSC–derived osteochondral progenitor cells to chondrogenesis (46). Deficiency for β-catenin in limb and head mesenchyme causes the formation of chondrocytes instead of osteoblasts (55, 63). These findings are in line with our in vivo and in vitro findings in *Yap* and *Taz*–deficient models. In addition, similar to Yap and Taz in NCCs and Yap in bmMSCs, the function of β-catenin in bmMSC–derived osteoblast formation is also stage-dependent, whereby the activation of the Wnt-β-catenin signaling pathway promotes bmMSC proliferation but represses osteoblastic differentiation (64, 65). After bmMSCs are committed to an osteoblast fate, the Wnt-β-catenin pathway promotes osteoblast differentiation (66-68). Here, we found that Yap and Taz in NCCs functioned in a stage-dependent manner similar to the Wnt-β-catenin signaling pathway in bmMSCs. Studies have indicated that crosstalk occurs between the Hippo and Wnt signaling pathways in biological processes such as the maintenance of intestinal stem cells in mice (69) and neural crest emigration in avian embryos (35). Yap and Taz can interact with β-catenin either in the nucleus, such as in the embryonic mouse heart (70), or in the cytoplasm, such as in the ST-2 MSC cell line (71). Our results showed that Yap and Taz interacted with β-catenin in NCCs, but we did not determine whether this interaction was direct or mediated by other members of a larger complex. Our findings support that the Yap/Taz-TEAD complex interacts with the Tcf/Lef-β-catenin complex in NCCs to regulate genes in a coordinated fashion. Yap and Taz promote osteogenesis by preventing chondrogenesis partly through this interaction with β-catenin; however, additional studies are needed to gain deeper insight into other mechanisms for how Yap and Taz function in this process. Our findings in NCCs may also have implications for bmMSCs and other types of stem cells.

MATERIALS AND METHODS

Transgenic mouse lines and alleles

The *Wnt1-Cre2*, $Yap^{-/-}$, $Taz^{-/-}$ and $mTmG^{-/-}$ mouse lines and alleles were previously described (41, 72-74). The mTmG mice (JAX Stock 007676) (42) were obtained from Jackson Laboratories. All mice were maintained in the animal facility of the University of Texas Health Science Center at Houston. The experimental protocol was reviewed and approved by the Animal Welfare Committee (AWC) and the Institutional Animal Care and Use Committee of the University of Texas Health Science Center at Houston (AWC-22-0049).

Radiographs and Micro-CT analysis

Radiographs were obtained by Kubtec XPERT80 (Kubtec X-ray, Milford, CT). The hair and skin of the mouse heads were removed, and the head samples were washed using PBS. Then

the skull samples were placed into a 16 mm tube filled with 70% ethanol and scanned using a SCANCO μCT 40 scanner.

Whole-mount skeletal staining

Heads of mutant mice and WT littermates from timepoints E18.5 and P5 were fixed in 95% ethanol overnight at 4 °C after the removal of skin and were transferred to acetone overnight at room temperature. Then, heads were incubated in a freshly prepared Alcian blue solution (0.015% Alcian blue in 80% ethanol and 20% acetic acid) (Sigma-Aldrich, A3157-10G) overnight at room temperature. Afterwards, the heads were rehydrated in 70% ethanol for 6 h at room temperature and cleared in 1% KOH overnight at room temperature, followed by immersion into freshly prepared Alizarin red solution (0.001% Alizarin red in 1% KOH) (Sigma-Aldrich, A5533-25G) for 3 days at room temperature. Then, the samples were cleared in 1% KOH and transferred to glycerol solution (50% glycerol and 50% ethanol).

Safranin O staining

All embryos were fixed in 4% PFA overnight at 4 °C, dehydrated with gradient ethanol (70%, 95%, 100%), embedded into paraffin, and cut into 7-μm-thick sections. The slides were then deparaffinized with xylene and hydrated in gradient ethanol (100%, 95%, 80%, 70%, 50%) and distilled water, stained with 1% fast green solution (Sigma-Aldrich, F7258-25G) for 5 min, and washed in 1% acetic acid for 10 s at room temperature. Next, the samples were stained for 25 min in 1% Safranin O solution (Sigma-Aldrich, S8884-25G) and dehydrated with 95% and 100% ethanol. Finally, the slides were transferred into xylene and mounted with mounting medium (Fisher Scientific, SP15-500). All images were acquired by using a LAS X imaging system (Leica).

Von Kossa staining

All embryos were fixed in 4% PFA overnight at 4 °C, dehydrated with gradient ethanol (70%, 95%, 100%), embedded into paraffin, and cut into 7-μm-thick sections. The slides were deparaffinized and hydrated in gradient ethanol (100%, 70%, 50%) and distilled water. Next, we stained the slides using a Von Kossa staining kit (Abcam; ab150687) according to the manufacturer's guidelines. Briefly, the slides were incubated in 1% silver nitrate solution for 30 min under ultraviolet light and 5% sodium thiosulfate for 5 min and were then rinsed with water and 3% acetic acid. The slides were next counterstained with nuclear fast red (Sigma-Aldrich, N8002-5G) for 5 min. After rinsing the slides with water, they were dehydrated with a gradient of ethanol (30%, 50%, 70%, 100%) and xylene and were mounted by using mounting medium (Fisher Scientific, SP15-500). Images were acquired by using a LAS X imaging system (Leica).

O9-1 cell culture and manipulation

O9-1 cells were a gift from Robert E. Maxson lab and were cultured under nondifferentiation conditions according to a previously described protocol (37). The conditions used for osteoblast differentiation were also described previously (38). For the siRNA-mediated KD experiments, O9-1 cells were transfected with siRNA SMART pools of *Yap* (Dharmacon, L-046247-01-0005), *Taz* (Dharmacon, L-041057-01), or scramble siRNA

(Dharmacon, D-001810-04-05) according to the guidelines of the RNAiMAX transfection procedure (Life Technologies, 13778075). For *Yap* KO O9-1 cells, exon 3 of *Yap* was deleted by using CRISPR/Cas9 genome editing as previously described (36). Cell lines were tested for mycoplasma contaminants.

Alizarin red staining

Ten days after differentiation, cells were washed twice with PBS, fixed in 4% PFA for 10 min at room temperature, and washed with PBS. Next, the cells were stained with 2% Alizarin red solution (pH 4.2) (Sigma-Aldrich, A5533-25G) for 30 min at room temperature and washed with water. Images were acquired by using a LAS X imaging system (Leica).

Alcian blue staining

Ten days after differentiation, cells were washed twice with PBS, fixed in 4% PFA for 10 min at room temperature, and washed with PBS. Next, the cells were stained in 1% Alcian blue solution (Sigma-Aldrich, A3157-10G) for 2 h at room temperature and rinsed three times with PBS. Subsequently, the cells were stored in PBS. All images were acquired by using an LAS X imaging system (Leica).

Ex vivo cell culture and differentiation

NCC-derived MSCs were harvested and dissociated from E13.5 embryonic frontal suture, and then cultured following protocol previously described (63). Briefly, suture tissue was minced by using fine-tipped dissecting scissors and digested in HBSS supplemented with 0.5% collagenase (Sigma-Aldrich, 10269638001) and 0.25% dextrose (Sigma-Aldrich, G8769) at 37 °C for 1 h. The cells were dissociated by gentle pipetting, spun down, and resuspended in BGJb medium supplemented with 10% fetal bovine serum (FBS) and 1% penicillin-streptomycin. The cells were expanded on a Matrigel-coated plate in a standard cell culture incubator (37 °C, 5% CO_2). After 48 h of culture, the cells were detached by using 0.25% trypsin, spun down, and plated in 24-well plates at 15,000 cells/cm^2. Differentiation was induced on day 1 by changing the culture medium to osteoblast differentiation medium as described previously (37). Cells were transfected with siRNA SMART pools of Yap (Dharmacon, L-046247-01-0005)/Taz (Dharmacon, L-041057-01) or and scramble siRNA (Dharmacon, D-001810-04-05), respectively, according to the guidelines of the RNAiMAX transfection procedure (Life Technologies, 13778075). The cells were grown for 21 days, and the differentiation medium was changed every other day.

Histologic analysis and immunofluorescence staining

All embryos were dissected in phosphate-buffered saline (PBS) and fixed in 4% paraformaldehyde (PFA) overnight at 4 °C. The embryos were processed and sectioned into 7-μm thick paraffin sections as described previously (36). Hematoxylin and eosin staining and immunofluorescence staining of paraffin sections were performed as previously described. Primary antibodies used for immunofluorescence staining were as follows: Sox9 (1:250, Abcam; ab185966), Sox5 (1:200, Abcam; ab94396), Sox6 (1:200, Abcam; ab30455), Runx2 (1:200, Santa Cruz; sc-390351), Col2a1 (1:500, Invitrogen; MA5-12789),

and GFP (1:500, Abcam; ab6673). Slides were visualized by using a LAS X imaging System (Leica).

Coimmunoprecipitation and Western blotting

To study the interaction between Yap and β-catenin, we performed coimmunoprecipitation experiments with WT and *Yap*/*Taz* dKD O9-1 cells. O9-1 cells were plated at 50% confluency in conditioned basal media. When the confluency reached 80%, cells were transfected with siRNAs as described above. The siRNA-transfected cells were harvested and lysed by using 0.5% NP-40 lysis buffer (50mM Tris-HCl [pH 7.5], 150mM NaCl, 0.5% NP-40, 10% glycerol, and phosphatase and protease inhibitors) for 1 h at 4 °C and centrifuged at 14,000 rpm for 10 minutes at 4 °C. The extracts of cells were collected and incubated with anti-Yap antibody (Novus, NB110-58358) or anti-rabbit-IgG antibody (Millipore Sigma, 12370) overnight at 4 °C. Next, Protein G Dynabeads (Invitrogen, 10003D) were added to the extracts. The immunocomplexes were washed 4 times with 1 mL of cold 0.5% NP-40 lysis buffer after 1 h of incubation. The immunocomplexes were then collected in 20 μL of 2X Laemmli sample buffer (Bio-Red, 1610747) supplemented with 2-mercaptoethanol (Bio-Red, 1610710). Subsequently, the samples were heated for 5 min at 100 °C.

For Western blot analysis, the proteins were separated by using sodium dodecyl sulfate polyacrylamide gel electrophoresis (SDS-PAGE; 5% stacking gel and 10% separating gel). The bands were transferred onto a PVDF membrane (Millipore, IPVH00010) and blocked in 5% milk for 1 h at room temperature. Next, the membrane was incubated with different primary antibodies overnight at 4 °C and then incubated with horse radish peroxidase (HRP)-conjugated secondary antibodies at a dilution of 1:3000. Protein bands were visualized by using a Clarity Western ECL Substrate kit (Bio-Rad, 1705061) and imaged with a Biorad imaging system. Relative protein levels were quantified by using ImageJ software (https://imagej.net/). To normalize for transfection efficiency, we loaded 0.5% inputs. Coimmunoprecipitation experiments were performed using anti-Yap antibody (Novus, NB110-58358) and anti-rabbit-IgG antibody (Millipore Sigma, 12370). Primary antibodies used in Western blotting were anti-Yap/Taz antibody (Cell Signaling Technology, 8418, 1:1,000), anti-β-catenin antibody (BD Transduction Laboratories, 610153, 1:1,000), anti-GAPDH antibody (Abcam, ab9485, 1:5000), anti-Sox9 antibody (Abcam, ab185966, 1:3000), anti-Sox2 antibody (Abcam, ab97959), anti-collagen II antibody (Invitrogen, MA5-12789, 1:200), anti-ALP antibody (Abcam, ab108337, 1:10000), and anti-Runx2 antibody (Santa Cruz, sc-390351, 1:100).

CUT&RUN and CUT&Tag sequencing

Cleavage under targets and release using nuclease (CUT&RUN) and cleavage Under Targets & tagmentation (CUT&Tag) experiments were performed according to the guidelines of previously published protocols (75) (76). Briefly, collected cells were immobilized on concanavalin A–coated magnetic beads (Bangs Laboratories, BP531), permeabilized with digitonin, and incubated with Yap1 (Novus, NB110-58358, 1:50), tri-methyl-histone H3 (Lys27) (Cell Signaling Technology, 9733, 1:50), and anti-rabbit IgG (Millipore Sigma, 12370, 1:50) antibodies separately overnight at 4 °C. Protein A/G–micrococcal nuclease

(pA/G-MNase) fusion protein was added into each sample to a final concentration of 700 ng/mL for 10 min at room temperature after washing away unbound antibodies. Next, we washed the samples with digitonin buffer and then added 150 μL digitonin buffer that was prechilled on ice, and $CaCl_2$ was added to a final concentration of 2 mM to activate the pAG-MNase enzyme for DNA digestion. After 2 h of digestion at 4 °C, the reactions were terminated by the addition of 100 uL STOP buffer, and the protein-DNA complexes were released by incubating the tubes at 37 °C for 10 min on a ThermoMixer at 500 rpm. Finally, DNA fragments were extracted by phenol-chloroform and ethanol and quantified by Qubit analysis according to the manufacturer's instructions (ThermoFisher Scientific, Q32851). pA/G-MNase was a generous gift from Dr. Steven Henikoff. CUT&RUN libraries were prepared by using the SMARTer® ThruPLEX® DNA-seq Kit (Takara Bio Inc, R400674) according to the manufacturer's instructions and were sequenced with paired-end 50-bp reads on an Illumina NovaSeq 6000 instrument.

CUT&Tag builds on the CUT&RUN protocol (76). It uses Tn5 transposase instead of MNase in CUT&RUN. The CUT&Tag assay was performed according to the guidelines of previously published protocol. Briefly, nuclei from O9-1 cells were incubated with concanavalin A (Con A)-coated magnetic beads (Bangs Laboratories, BP531) at room temperature for 10 min to immobilize the nuclei on the Con A-coated magnetic beads. The bead-bound nuclei were then incubated with antibodies overnight at 4 °C with rotation. Guinea pig anti-rabbit secondary antibody (Antibodies-Online, ABIN101961, 1:100) was added to the nuclei and incubated for 30 min at room temperature. The pA-Tn5 adapter complex was incubated with nuclei at room temperature for 1 h. Nuclei were then resuspended in tagmentation buffer at 37 °C for 1 h for DNA fragmentation. After 1 h, 0.5 M EDTA, 10% SDS, and 20 mg/mL proteinase K were added to terminate tagmentation and incubate for 10 min at 70 °C. DNA was then purified by using phenol-chloroform-isoamyl alcohol extraction and ethanol precipitation and dissolved in 21 μL 1 mM Tris-HCl (pH=8) and 0.1 mM EDTA.

Sequencing data processing and analysis

For ATAC-seq data,, the FASTQ format raw reads were aligned to reference genome by Bowtie2 (77) with the parameter setting of "--very-sensitive". SAMtools (78) were used for filtering the nonuniquely mapped reads and low mapping quality reads, and the mitochondrial reads and PCR duplicates were removed by Picard with the function of "MarkDuplicates". The bigwig file was generated for UCSC visualization. Then, MACS2 (79) took the alignment files produced in the previous step as input to call peaks. The setting was "--keep-dup all".. HOMER (80) software was used for de novo motif analysis of peaks. The overlapping peaks were identified by using bedtools (79), with a minimum overlap of 1 bp. Then, the number for each set was deposited into Rpackage "Vennerable" to generate a Venn plot. The GREAT (81) tool was used to predict the genes associated with the TEAD and TCF/LEF motif binding sites. Metascape (82) was used in Gene Ontology (GO) and Kyoto Encyclopedia of Genes and Genomes (KEGG) pathway analysis.

For CUT&RUN data processing, FASTQ format raw reads were aligned to mm10 and *E. coli* reference genomes by Bowtie2 (77) with the setting of "--local --very-sensitive-local

--no-unal --no-mixed --no-discordant --phred33 -I 10 -X 700", separately. Then, the mm10 alignment files were normalized with the associated *E. coli* spike alignments (83), and the bigwigs were generated for University of California Santa Cruz (UCSC) genome browser visualization. The normalized alignment files were used to call peaks by MACS2 (79) with the parameters of "-q 0.01 -B --SPMR --keep-dup all", and the IgG sample was used as a control. The output narrowPeak file was then annotated by the "annotatePeaks" function of HOMER (80), and the compositions of peaks were calculated to generate a pie plot. R package "Gennomation" was used to produce the signal heatmap. The YAP peaks were scaled by using the 2-kb region around the peak summit and were used to profile the heatmap. Additionally, processed dataset was performed for GO analysis by using Metascape, which provided multiple defined terms that represented gene properties such as cellular component, molecular function, and biological processes. For CUT&Tag, FASTQ format raw reads were aligned to mm10 by Bowtie2 with the setting of "--local --very-sensitive-local --no-unal --no-mixed --no-discordant --phred33 -I 10 -X 700", separately. The bigwigs were generated for University of California Santa Cruz (UCSC) genome browser visualization. The alignment files were used to call peaks by SEACR with the parameters of "norm stringent". The output stringent peaks files were then annotated by the R package "ChIPseeker".

Proximity ligation assay (PLA)

We performed the PLA in O9-1 cells by using the Duolink™ In Situ Red Starter Kit according to the manufacturer's guidelines (Sigma-Aldrich DUO92101). Briefly, O9-1 cells were plated on 24-well plates, cultured in basal medium or osteoblast differentiation medium for 48 h, and fixed with 4% paraformaldehyde for 10 min at room temperature. Then, the cells were permeabilized in PBS/Triton 0.5% for 15 min at room temperature and blocked for 1 h in Duolink® blocking solution at 37 °C. After this, the cells were incubated with primary antibodies against Yap (1:100, Santa Cruz; sc-101199) and β-catenin (1:200, Cell signaling; 9562) overnight at 4 °C. Next, the cells were incubated with the proximity ligation assay probes (1 h), ligase (30 min), and polymerase (100 min) at 37 °C. After washing the cells, they were mounted by using the Duolink® In Situ Mounting Medium with DAPI. Red fluorescence indicated the association of Yap and β-catenin in cells. To control for nonspecific fluorescence background, each primary antibody was used alone. Slides were visualized by using a LAS X imaging system (Leica).

Quantification and statistical analysis

ImageJ software was used for cell counting and intensity analysis of immunofluorescence images, and for the grey intensity analysis of Western blot results. For immunofluorescence data of O9-1 NCCs, we analyzed the ratio of Ocn^+, $Col2a1^+$ and $Col1a1^+$ cells by using Ocn^+, $Col2a1^+$ or $Col1a1^+$ cell number to divide by the total cell number (DAPI); we analyzed the mean intensity of Runx2 and Sox9 signaling in different groups and then expressed these data as fold change relative to their respective control. For the difference between two compared groups, two-sample *t* tests were used for the data conforming to normal distribution and Mann-Whitney test was used for data not normally distributed, as indicated in the figure legends. For more than two comparable groups, one-way ANOVA with post-hoc Tukey's tests were used for the data conforming to normal distribution, and

Kruskal-Wallis tests with *post-hoc* Dunn's tests were used for not normally distributed data as indicated in the figure legends. Western blot data were relative to their respective control and were analyzed by one-sample *t* tests. qRT-PCR data were analyzed using Mann-Whitney tests. All tests were two-tailed, and all assumptions of normality were assessed using Shapiro-Wilks tests. A *p*-value (p) ≤0.05 was considered statistically significant. In the figures, * denotes $p < 0.05$, ** denotes $p < 0.01$, and *** denotes $p < 0.001$. All quantification data were presented as the mean ± standard error of the mean (SEM). All bar graphs and statistical analyses were performed using GraphPad Prism version 8.0.

Supplementary Material

Refer to Web version on PubMed Central for supplementary material.

Acknowledgments

We thank Dr. Nicole Stancel, ELS (D) for editorial assistance with the manuscript, and Kaleigh L. Riggs from University of Texas health science center at Houston for assisting with statistical analysis. We thank Dr. Jianning Tao and the Center for Skeletal Medicine and Biology at Baylor College of Medicine for technical support. We also thank the technical support from Cancer Genomics Center supported by the Cancer Prevention and Research Institute of Texas (CPRIT RP180734).

Funding

We thank the funding sources from the National Institutes of Health (K01DE026561, R03DE025873, R01DE029014, R56HL142704, and R01HL142704 to Jun Wang; the Lawrence Research Award from the Rolanette and Berdon Lawrence Bone Disease Program of Texas (to Jun Wang).

REFERENCES AND NOTES

1. Hoppler S, Wheeler GN, DEVELOPMENTAL BIOLOGY. It's about time for neural crest. Science 348, 1316–1317 (2015). [PubMed: 25931447]
2. Baggiolini A et al. , Premigratory and migratory neural crest cells are multipotent in vivo. Cell Stem Cell 16, 314–322 (2015). [PubMed: 25748934]
3. Jiang X, Iseki S, Maxson RE, Sucov HM, Morriss-Kay GM, Tissue origins and interactions in the mammalian skull vault. Dev Biol 241, 106–116 (2002). [PubMed: 11784098]
4. Chai Y, Maxson RE Jr., Recent advances in craniofacial morphogenesis. Dev. Dyn 235, 2353–2375 (2006). [PubMed: 16680722]
5. Dash S, Trainor PA, The development, patterning and evolution of neural crest cell differentiation into cartilage and bone. Bone 137, 115409 (2020). [PubMed: 32417535]
6. Sauka-Spengler T, Bronner-Fraser M, A gene regulatory network orchestrates neural crest formation. Nat Rev Mol Cell Biol 9, 557–568 (2008). [PubMed: 18523435]
7. Wang J, Liu S, Heallen T, Martin JF, The Hippo pathway in the heart: pivotal roles in development, disease, and regeneration. Nat Rev Cardiol, (2018).
8. Wang J, Martin JF, Hippo Pathway: An Emerging Regulator of Craniofacial and Dental Development. J Dent Res 96, 1229–1237 (2017). [PubMed: 28700256]
9. Lachowski D et al. , FAK controls the mechanical activation of YAP, a transcriptional regulator required for durotaxis. The FASEB Journal 32, 1099–1107 (2018). [PubMed: 29070586]
10. Li C-Y et al. , αE-catenin inhibits YAP/TAZ activity to regulate signalling centre formation during tooth development. Nature communications 7, 1–13 (2016).
11. Silvis MR et al. , α-catenin is a tumor suppressor that controls cell accumulation by regulating the localization and activity of the transcriptional coactivator Yap1. Science signaling 4, ra33–ra33 (2011). [PubMed: 21610251]

12. Moon S et al. , Phosphorylation by NLK inhibits YAP-14-3-3-interactions and induces its nuclear localization. EMBO reports 18, 61–71 (2017). [PubMed: 27979972]
13. Zhang W et al. , VGLL4 functions as a new tumor suppressor in lung cancer by negatively regulating the YAP-TEAD transcriptional complex. Cell research 24, 331–343 (2014). [PubMed: 24458094]
14. Cordenonsi M et al. , The Hippo transducer TAZ confers cancer stem cell-related traits on breast cancer cells. Cell 147, 759–772 (2011). [PubMed: 22078877]
15. Hong JH et al. , TAZ, a transcriptional modulator of mesenchymal stem cell differentiation. Science 309, 1074–1078 (2005). [PubMed: 16099986]
16. Mo JS, Park HW, Guan KL, The Hippo signaling pathway in stem cell biology and cancer. EMBO Rep 15, 642–656 (2014). [PubMed: 24825474]
17. Tang Y, Feinberg T, Keller ET, Li XY, Weiss SJ, Snail/Slug binding interactions with YAP/TAZ control skeletal stem cell self-renewal and differentiation. Nat Cell Biol 18, 917–929 (2016). [PubMed: 27479603]
18. Heng BC et al. , Role of YAP/TAZ in Cell Lineage Fate Determination and Related Signaling Pathways. Front Cell Dev Biol 8, 735 (2020). [PubMed: 32850847]
19. Park JS et al. , A reciprocal role of the Smad4-Taz axis in osteogenesis and adipogenesis of mesenchymal stem cells. Stem Cells 37, 368–381 (2019). [PubMed: 30444564]
20. Dupont S et al. , Role of YAP/TAZ in mechanotransduction. Nature 474, 179–183 (2011). [PubMed: 21654799]
21. Pan J-X et al. , YAP promotes osteogenesis and suppresses adipogenic differentiation by regulating β-catenin signaling. Bone research 6, 1–12 (2018). [PubMed: 29423330]
22. Kegelman CD et al. , Skeletal cell YAP and TAZ combinatorially promote bone development. The FASEB Journal 32, 2706–2721 (2018). [PubMed: 29401582]
23. Seo E et al. , SOX2 regulates YAP1 to maintain stemness and determine cell fate in the osteo-adipo lineage. Cell reports 3, 2075–2087 (2013). [PubMed: 23791527]
24. Goto H et al. , Loss of Mob1a/b in mice results in chondrodysplasia due to YAP1/TAZ-TEAD-dependent repression of SOX9. Development 145, (2018).
25. Yang B et al. , YAP1 negatively regulates chondrocyte differentiation partly by activating the β-catenin signaling pathway. The international journal of biochemistry & cell biology 87, 104–113 (2017). [PubMed: 28438716]
26. Karystinou A et al. , Yes-associated protein (YAP) is a negative regulator of chondrogenesis in mesenchymal stem cells. Arthritis research & therapy 17, 1–14 (2015). [PubMed: 25566937]
27. Deng Y et al. , Yap1 regulates multiple steps of chondrocyte differentiation during skeletal development and bone repair. Cell reports 14, 2224–2237 (2016). [PubMed: 26923596]
28. Li Y, Yang S, Qin L, Yang S, TAZ is required for chondrogenesis and skeletal development. Cell Discovery 7, 1–13 (2021). [PubMed: 33390590]
29. Vanyai HK et al. , Control of skeletal morphogenesis by the Hippo-YAP/TAZ pathway. Development 147, (2020).
30. Bi-Lin KW et al. , Critical role of the BAF chromatin remodeling complex during murine neural crest development. PLoS genetics 17, e1009446 (2021). [PubMed: 33750945]
31. Bhattacharya D, Azambuja AP, Simoes-Costa M, Metabolic reprogramming promotes neural crest migration via yap/tead signaling. Developmental cell 53, 199–211. e196 (2020). [PubMed: 32243782]
32. Zhao X et al. , Yap and Taz promote osteogenesis in neural crest cells by preventing chondrogenesis. The FASEB Journal 36, (2022).
33. Williamson KA et al. , Heterozygous loss-of-function mutations in YAP1 cause both isolated and syndromic optic fissure closure defects. The American Journal of Human Genetics 94, 295–302 (2014). [PubMed: 24462371]
34. Bonnard C et al. , A loss-of-function NUAK2 mutation in humans causes anencephaly due to impaired Hippo-YAP signaling. J Exp Med 217, (2020).

35. Kumar D, Nitzan E, Kalcheim C, YAP promotes neural crest emigration through interactions with BMP and Wnt activities. Cell Communication and Signaling 17, 1–17 (2019). [PubMed: 30616541]
36. Wang J et al. , Yap and Taz play a crucial role in neural crest-derived craniofacial development. Development 143, 504–515 (2016). [PubMed: 26718006]
37. Ishii M et al. , A stable cranial neural crest cell line from mouse. Stem cells and development 21, 3069–3080 (2012). [PubMed: 22889333]
38. Nguyen BH, Ishii M, Maxson RE, Wang J, Culturing and manipulation of O9-1 neural crest cells. JoVE (Journal of Visualized Experiments), e58346 (2018).
39. Masui S et al. , Pluripotency governed by Sox2 via regulation of Oct3/4 expression in mouse embryonic stem cells. Nature cell biology 9, 625–635 (2007). [PubMed: 17515932]
40. Yoshida T, Vivatbutsiri P, Morriss-Kay G, Saga Y, Iseki S, Cell lineage in mammalian craniofacial mesenchyme. Mechanisms of development 125, 797–808 (2008). [PubMed: 18617001]
41. Lewis AE, Vasudevan HN, O'Neill AK, Soriano P, Bush JO, The widely used Wnt1-Cre transgene causes developmental phenotypes by ectopic activation of Wnt signaling. Dev. Biol 379, 229–234 (2013). [PubMed: 23648512]
42. Muzumdar MD, Tasic B, Miyamichi K, Li L, Luo L, A global double-fluorescent Cre reporter mouse. genesis 45, 593–605 (2007). [PubMed: 17868096]
43. Prescott SL et al. , Enhancer divergence and cis-regulatory evolution in the human and chimp neural crest. Cell 163, 68–83 (2015). [PubMed: 26365491]
44. Minoux M et al. , Gene bivalency at Polycomb domains regulates cranial neural crest positional identity. Science 355, (2017).
45. Long HK et al. , Loss of extreme long-range enhancers in human neural crest drives a craniofacial disorder. Cell Stem Cell 27, 765–783. e714 (2020). [PubMed: 32991838]
46. Akiyama H, Chaboissier M-C, Martin JF, Schedl A, de Crombrugghe B, The transcription factor Sox9 has essential roles in successive steps of the chondrocyte differentiation pathway and is required for expression of Sox5 and Sox6. Genes Dev. 16, 2813–2828 (2002). [PubMed: 12414734]
47. Lee H-Y et al. , Instructive role of Wnt/ß-catenin in sensory fate specification in neural crest stem cells. Science 303, 1020–1023 (2004). [PubMed: 14716020]
48. Dorsky RI, Moon RT, Raible DW, Control of neural crest cell fate by the Wnt signalling pathway. Nature 396, 370–373 (1998). [PubMed: 9845073]
49. Hari L et al. , Lineage-specific requirements of β-catenin in neural crest development. The Journal of cell biology 159, 867–880 (2002). [PubMed: 12473692]
50. Santagati F, Rijli FM, Cranial neural crest and the building of the vertebrate head. Nature Reviews Neuroscience 4, 806–818 (2003). [PubMed: 14523380]
51. Xiong J, Almeida M, O'Brien CA, The YAP/TAZ transcriptional co-activators have opposing effects at different stages of osteoblast differentiation. Bone 112, 1–9 (2018). [PubMed: 29626544]
52. Zhao X, Le TP, Erhardt S, Findley TO, Wang J, Hippo-Yap Pathway Orchestrates Neural Crest Ontogenesis. Frontiers in Cell and Developmental Biology 9, (2021).
53. Setiawan I, Sanjaya A, Lesmana R, Yen PM, Goenawan H, Hippo pathway effectors YAP and TAZ and their association with skeletal muscle ageing. Journal of physiology and biochemistry 77, 63–73 (2021). [PubMed: 33495890]
54. Reggiani F, Gobbi G, Ciarrocchi A, Sancisi V, YAP and TAZ are not identical twins. Trends in Biochemical Sciences 46, 154–168 (2021). [PubMed: 32981815]
55. Hill TP, Später D, Taketo MM, Birchmeier W, Hartmann C, Canonical Wnt/β-catenin signaling prevents osteoblasts from differentiating into chondrocytes. Dev. Cell 8, 727–738 (2005). [PubMed: 15866163]
56. Schatten GP, Current topics in developmental biology. (Elsevier, 2007).
57. Bi W, Deng JM, Zhang Z, Behringer RR, de Crombrugghe B, Sox9 is required for cartilage formation. Nat Genet 22, 85–89 (1999). [PubMed: 10319868]

58. Lefebvre V, Behringer RR, de Crombrugghe B, L-Sox5, Sox6 and Sox9 control essential steps of the chondrocyte differentiation pathway. Osteoarthritis Cartilage 9 Suppl A, S69–75 (2001). [PubMed: 11680692]
59. Mori-Akiyama Y, Akiyama H, Rowitch DH, de Crombrugghe B, Sox9 is required for determination of the chondrogenic cell lineage in the cranial neural crest. Proceedings of the National Academy of Sciences 100, 9360–9365 (2003).
60. Mundlos S et al. , Mutations involving the transcription factor CBFA1 cause cleidocranial dysplasia. Cell 89, 773–779 (1997). [PubMed: 9182765]
61. Shirai Y et al. , Runx2 function in cells of neural crest origin during intramembranous ossification. Biochemical and biophysical research communications 509, 1028–1033 (2019). [PubMed: 30660360]
62. Gaur T et al. , Canonical WNT signaling promotes osteogenesis by directly stimulating Runx2 gene expression. Journal of Biological Chemistry 280, 33132–33140 (2005). [PubMed: 16043491]
63. Day TF, Guo X, Garrett-Beal L, Yang Y, Wnt/β-catenin signaling in mesenchymal progenitors controls osteoblast and chondrocyte differentiation during vertebrate skeletogenesis. Developmental cell 8, 739–750 (2005). [PubMed: 15866164]
64. Boland GM, Perkins G, Hall DJ, Tuan RS, Wnt 3a promotes proliferation and suppresses osteogenic differentiation of adult human mesenchymal stem cells. Journal of cellular biochemistry 93, 1210–1230 (2004). [PubMed: 15486964]
65. De Boer J et al. , Wnt signaling inhibits osteogenic differentiation of human mesenchymal stem cells. Bone 34, 818–826 (2004). [PubMed: 15121013]
66. Kahler RA et al. , Collagen 11a1 is indirectly activated by lymphocyte enhancer-binding factor 1 (Lef1) and negatively regulates osteoblast maturation. Matrix Biol. 27, 330–338 (2008). [PubMed: 18280717]
67. Rodda SJ, McMahon AP, Distinct roles for Hedgehog and canonical Wnt signaling in specification, differentiation and maintenance of osteoblast progenitors. Development 133, 3231–3244 (2006). [PubMed: 16854976]
68. Goodnough LH et al. , Distinct requirements for cranial ectoderm and mesenchyme-derived wnts in specification and differentiation of osteoblast and dermal progenitors. PLoS Genet 10, e1004152 (2014). [PubMed: 24586192]
69. Li Q et al. , Lats1/2 Sustain Intestinal Stem Cells and Wnt Activation through TEAD-Dependent and Independent Transcription. Cell Stem Cell, (2020).
70. Heallen T et al. , Hippo pathway inhibits Wnt signaling to restrain cardiomyocyte proliferation and heart size. Science 332, 458–461 (2011). [PubMed: 21512031]
71. Azzolin L et al. , YAP/TAZ incorporation in the beta-catenin destruction complex orchestrates the Wnt response. Cell 158, 157–170 (2014). [PubMed: 24976009]
72. Chai Y et al. , Fate of the mammalian cranial neural crest during tooth and mandibular morphogenesis. Development 127, 1671–1679 (2000). [PubMed: 10725243]
73. Xin M et al. , Hippo pathway effector Yap promotes cardiac regeneration. Proceedings of the National Academy of Sciences 110, 13839–13844 (2013).
74. Xin M et al. , Regulation of insulin-like growth factor signaling by Yap governs cardiomyocyte proliferation and embryonic heart size. Science signaling 4, ra70–ra70 (2011). [PubMed: 22028467]
75. Skene PJ, Henikoff JG, Henikoff S, Targeted in situ genome-wide profiling with high efficiency for low cell numbers. Nature protocols 13, 1006–1019 (2018). [PubMed: 29651053]
76. Kaya-Okur HS, Janssens DH, Henikoff JG, Ahmad K, Henikoff S, Efficient low-cost chromatin profiling with CUT&Tag. Nature protocols 15, 3264–3283 (2020). [PubMed: 32913232]
77. Langmead B, Salzberg SL, Fast gapped-read alignment with Bowtie 2. Nature methods 9, 357–359 (2012). [PubMed: 22388286]
78. Li H et al. , The sequence alignment/map format and SAMtools. Bioinformatics 25, 2078–2079 (2009). [PubMed: 19505943]
79. Zhang Y et al. , Model-based analysis of ChIP-Seq (MACS). Genome biology 9, 1–9 (2008).

80. Heinz S et al. , Simple combinations of lineage-determining transcription factors prime cis-regulatory elements required for macrophage and B cell identities. Molecular cell 38, 576–589 (2010). [PubMed: 20513432]

81. McLean CY et al. , GREAT improves functional interpretation of cis-regulatory regions. Nature biotechnology 28, 495–501 (2010).

82. Zhou Y et al. , Metascape provides a biologist-oriented resource for the analysis of systems-level datasets. Nature communications 10, 1–10 (2019).

83. Chen K et al. , The overlooked fact: fundamental need for spike-in control for virtually all genome-wide analyses. Molecular and cellular biology 36, 662–667 (2015). [PubMed: 26711261]

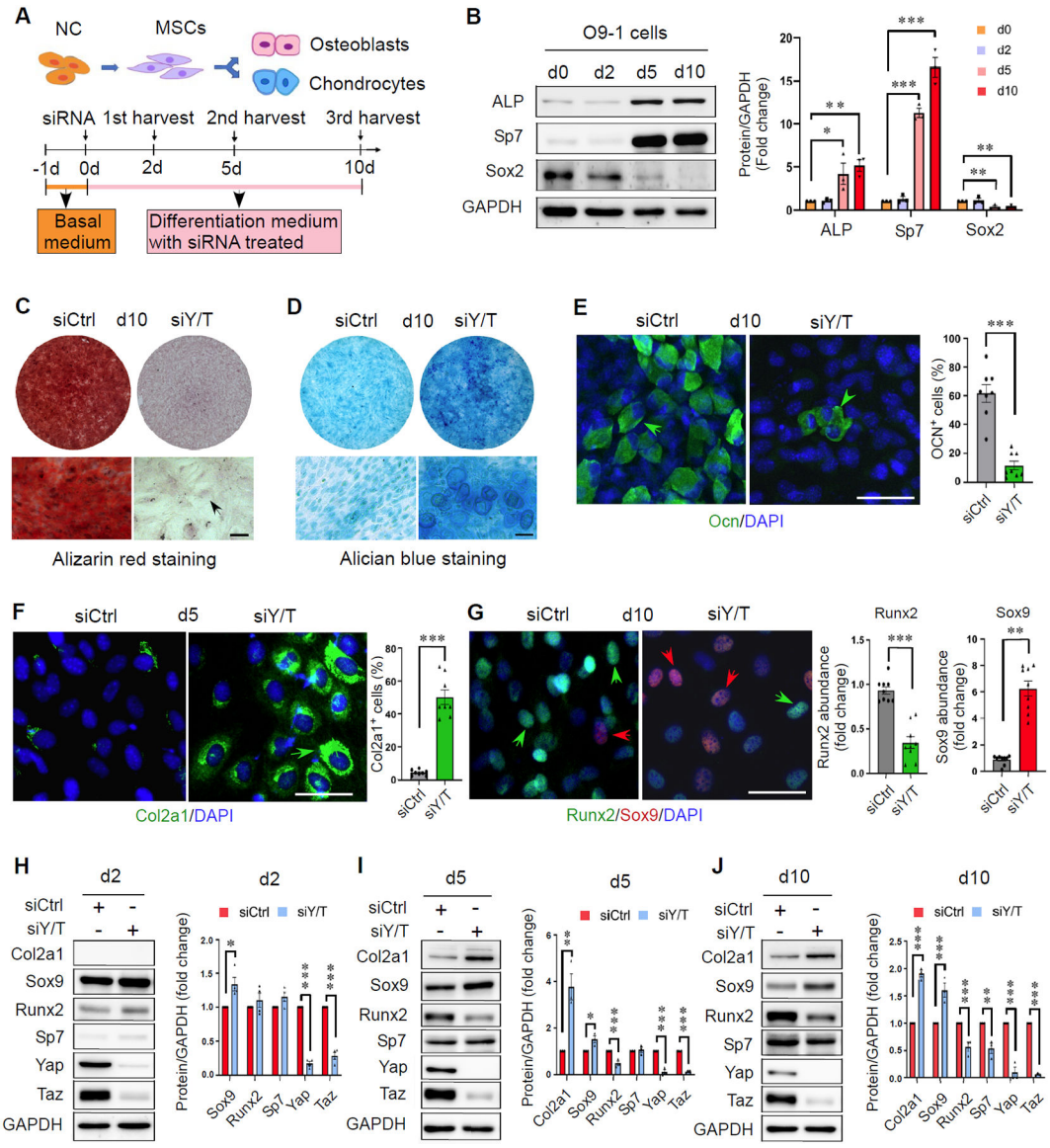

Fig 1. Yap and Taz promote osteogenesis and repress chondrogenesis in NCCs.

(A) Strategy used to study the functions of Yap and Taz in O9-1 NCCs at different days (d) of osteoblast differentiation. **(B)** Western blot analysis and quantification of the osteogenic markers ALP and Sp7 and the stemness marker Sox2 in O9-1 cells at the indicated time points during culture in osteoblast differentiation medium. GAPDH is a loading control. n = 3 independent experiments. (**C and D**) Representative images of Alizarin red (C) and Alcian blue (D) staining in control (siCtrl) and *Yap* and *Taz* double knockdown (siY/T) O9-1 NCCs at d10. Images are representative of 4 (C) or 3 (D) independent experiments. Scale bar, 50 μm. (**E to G)** Representative images and quantification of Ocn (E), Col2a1 (F), or Runx2 and Sox9 (G) in siCtrl and siY/T O9-1 NCCs at d5 or d10 as indicated. Cells were counterstained with DAPI to label nuclei. n = 4 (E and F) or 3 (G) independent experiments, with 2 (E and F) or 3 (G) different fields analyzed in each independent experiment. Scale bars, 50 μm. (**H** to **J**) Western blot analysis and quantification of Yap, Taz, osteogenic

markers (Runx2 and Sp7), and chondrogenic markers (Sox9 and Col2a1) in siCtrl and siY/TO9-1 NCCs at d2 (H), d5 (I), and d10 (J). For d2, n = 4 independent experiments. For d5 and d10, n = 3 independent experiments. The fold-change is shown relative to d0 for (B) or siCtrl for (G), (H), (I), and (J). All quantitative data are expressed as the mean ± SEM. For (B), one-way analysis of variance (ANOVA) combined with Tukey's multiple comparisons test was used. For (E), (F), and Runx2 quantification in G, unpaired *t* test was used. For Sox9 quantification in G, the Mann-Whitney test was used. For (H), (I), and (J), the one-sample *t* test was used. $*p < 0.05$, $**p < 0.01$, $***p < 0.001$.

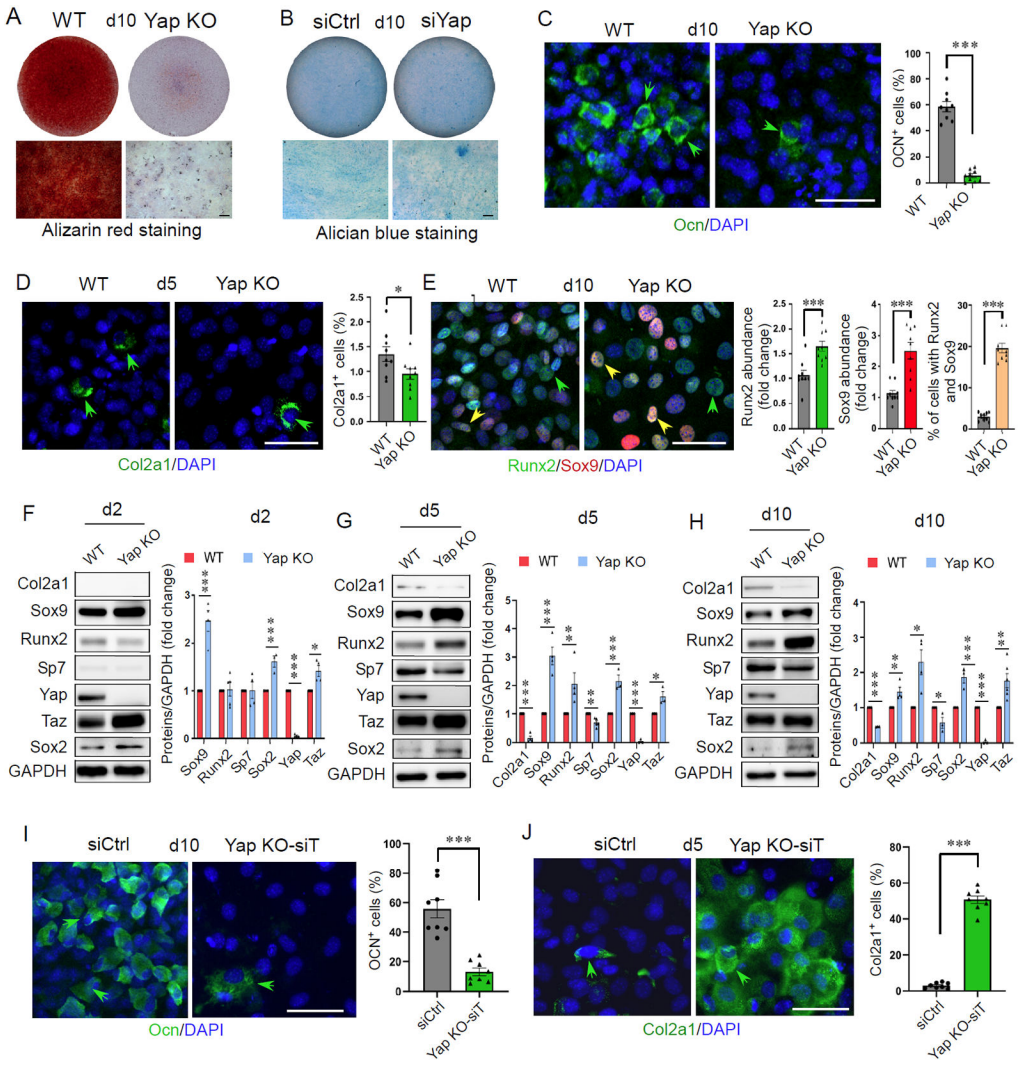

Fig 2. *Yap* deficiency arrests osteochondral development in vitro.

(**A**) Alizarin red staining of wild-type (WT) and *Yap* knockout (KO) NCCs at day (d) 10 in osteogenic differentiation culture. Data are representative of 3 independent experiments. Scale bar, 50 μm. (**B**) Alcian blue staining of control (siCtrl) and *Yap* knockdown (siYap) NCCs at d10. Data are representative of 3 independent experiments. Scale bar, 50 μm. (**C to E**) Immunofluorescence imaging and quantification of Ocn (C), Col2a1 (D), or Runx2 and Sox9 (E) in WT and *Yap* KO NCCs at the indicated time points. Cells were counterstained with DAPI to label nuclei. Each set of data is representative of n = 3 independent experiments. Three different fields in each independent experiment were analyzed. Scale bars, 50 μm. (**F to H**) Western blotting and quantification of the indicated proteins in WT and *Yap* KO O9-1 NCCs at d2 (F), d5 (G), and d10 (H). GAPDH is a loading control. For d2, d5 and d10, n = 3 to 6 biological replicates from 3 to 4 independent experiments. (**I and J**) Representative images and quantification of Ocn (I) or Col2a1 (J) in siCtrl and *Yap* KO with *Taz* KD (*Yap* KO-siT) O9-1 NCCs at the indicated time points. Each set of data represents 4 independent experiments. Two different fields in each independent experiment were analyzed. Scale bar, 50 μm. All quantification data are shown as the mean ± SEM. Data

are expressed as the fold-change relative to WT for Runx2 and Sox9 abundance in (E), (F), (G), and (H). For (C), (D), (E), (I), and (J), the unpaired *t* test was used. For (F), (G), and (H), one-sample *t* test was used. *$p < 0.05$, **$p < 0.01$, ***$p < 0.001$.

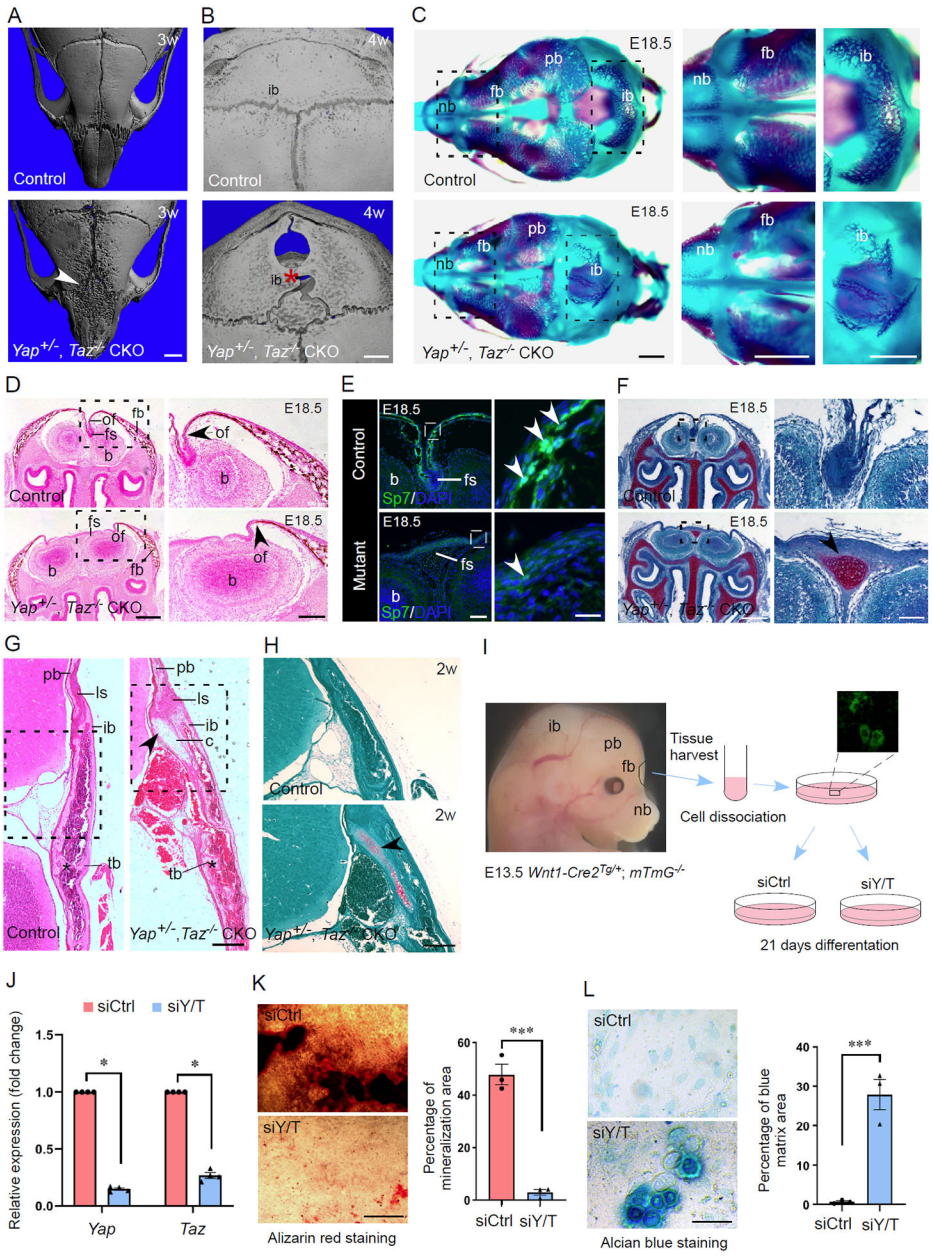

Fig 3. *Yap and Taz* deficiency in NCCs causes cranial bone defects and ectopic cartilage formation in vivo.

(A and **B)** Microcomputed tomography (μCT) imaging of skulls of 3 (A) and 4 (B)-week-old *Yap*$^{+/-}$;*Taz*$^{-/-}$ CKO mutants and *Wnt1-Cre2*$^{+/+}$;*Yap*$^{f/+}$;*Taz*$^{f/+}$ control littermates. White arrowheads indicate defective bone mineralization in NCC-derived nasal and frontal bones (A), and red asterisks indicate defective mineralization in interparietal bones (B). Scale bars, 1 mm (A) and 1 mm (B). (**C**) Whole-mount Alizarin red and Alcian blue staining in the cranial skeleton of E18.5 *Wnt1-Cre2*$^{+/+}$;*Yap*$^{f/f}$;*Taz*$^{f/f}$ control and *Yap*$^{+/-}$;*Taz*$^{-/-}$ CKO embryos. The NCC-derived nasal (nb), frontal (fb), and interparietal (ib) bones are labelled. Scale bars, 1 mm . (**D to F**) Von Kossa staining (D), immunofluorescence staining showing Sp7 (E), and Safranin O staining (F) in coronal sections through the frontal bone of E18.5

Cre-negative controls *Wnt1-Cre2*$^{+/+}$; *Yap*$^{f/f}$; *Taz*$^{f/+}$ (D), *Wnt1-Cre2*$^{+/+}$; *Yap*$^{f/+}$; *Taz*$^{f/+}$ (E), and *Wnt1-Cre2*$^{+/+}$; *Yap*$^{f/f}$; *Taz*$^{f/+}$ (F) and *Yap*$^{+/-}$; *Taz*$^{-/-}$ CKO mutant embryos. Black arrowheads in (D) point to osteogenic fronts. Write arrowheads in (E) point to Sp7^{+} cells. Black arrowhead in (F) points to ectopic cartilage in the metopic suture region. The sections in (E) were counterstained with DAPI to label nuclei. Scale bars, 500 μm (D, main images), 200 μm (D inserts), 100 μm (E, main images), 25 μm (E, inserts), 500 μm (F, main images), 50 μm (F, inserts) . (**G**) Representative images of hematoxylin and eosin (H&E) staining of sagittal sections from the interparietal bone regions of 2-week-old *Wnt1-Cre2*$^{+/+}$; *Yap*$^{f/+}$; *Taz*$^{f/f}$ control and *Yap*$^{+/-}$; *Taz*$^{-/-}$ CKO mutant mice. Black arrowhead points to ectopic cartilage (c); black asterisk notes defective trabecular bone (tb). Scale bar, 200 μm. (**H)** Safranin O staining in sagittal sections of interparietal bone regions in 2-week-old *Wnt1-Cre2*$^{+/+}$; *Yap*$^{f/+}$; *Taz*$^{f/f}$ control and *Yap*$^{+/-}$; *Taz*$^{-/-}$ CKO mutant mice. Black arrowhead points to ectopic cartilage. Scale bar, 100 μm. (**I)** Schematic showing the harvesting and processing of primary cells from the frontal suture region of E13.5 *Wnt1-Cre2*$^{Tg/+}$; *mTmG*$^{-/-}$ embryos. The NCC lineage is indicated by GFP expression (green). (**J**) Quantification of *Yap* and *Taz* transcripts relative to *Gapdh* in siCtrl and siY/T cells by qRT-PCR. (**K)** Alizarin red staining and quantification of mineralization at day 21 of differentiation of primary cells from E13.5 embryos treated with scrambled siRNA (siCtrl) or *Yap/Taz*-targeted siRNA (siY/T). Scale bar, 500 μm. (**L**) Alcian blue staining and quantification at day 21 of differentiation of primary cells from E13.5 embryos treated with siCtrl or siY/T. Scale bar, 50 μm. All images are representative of at least 3 independent experiments. The quantitative data for (J) represent 4 independent experiments, and for (K) and (L) represent 3 independent experiments. Quantitative data are shown as the mean ± SEM. Data are expressed as the fold-change relative to siCtrl for (J). For (J), the Mann-Whitney test was used. For (K) and (L), an unpaired *t* test was used. * $p < 0.05$, *** $p < 0.001$. b, brain; c, cartilage; fb, frontal bone; fs, frontal suture; ib, interparietal bone; ls, lambdoid suture; nb, nasal bone; of, osteogenic front; pb, parietal bone; tb, trabecular bone.

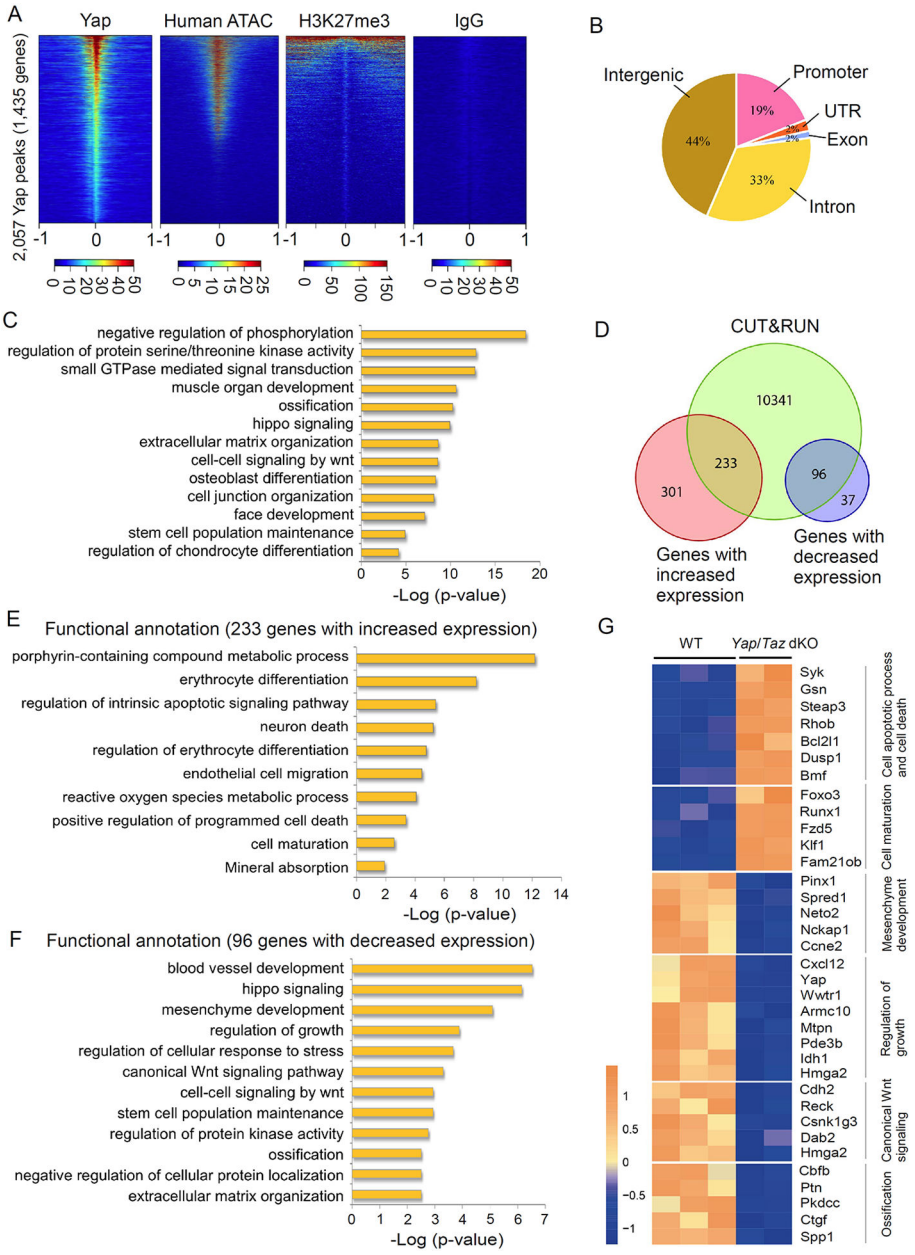

Fig 4. Direct target genes of Yap in NCCs.

(**A**) Heatmap showing Yap, IgG, and H3K27me3 DNA binding peaks determined by CUT&RUN sequencing in O9-1 cells and published human NCC ATAC-seq data (43). (**B**) Distribution of Yap-associated regions. (**C**) Gene ontology (GO) analysis of Yap-bound genes. (**D**) Venn diagram showing overlap of Yap-bound genes identified from CUT&RUN-seq with differentially regulated genes in published RNA-seq data from E10.5 mandibular tissues of *Yap/Taz* dCKO mutants compared with control embryos (36). (**E** and **F**) GO analysis of candidate direct Yap target genes including Yap-repressed genes (increase expression in *Yap/Taz* dCKO mutants) € and activated genes (decreased expression in *Yap/TAZ* dCKO mutants) (F). (**G**) Heatmap showing differentially increased and decreased

transcripts in E10.5 *Yap/TAZ* dCKO mutants versus control embryos that are candidate direct Yap target genes.

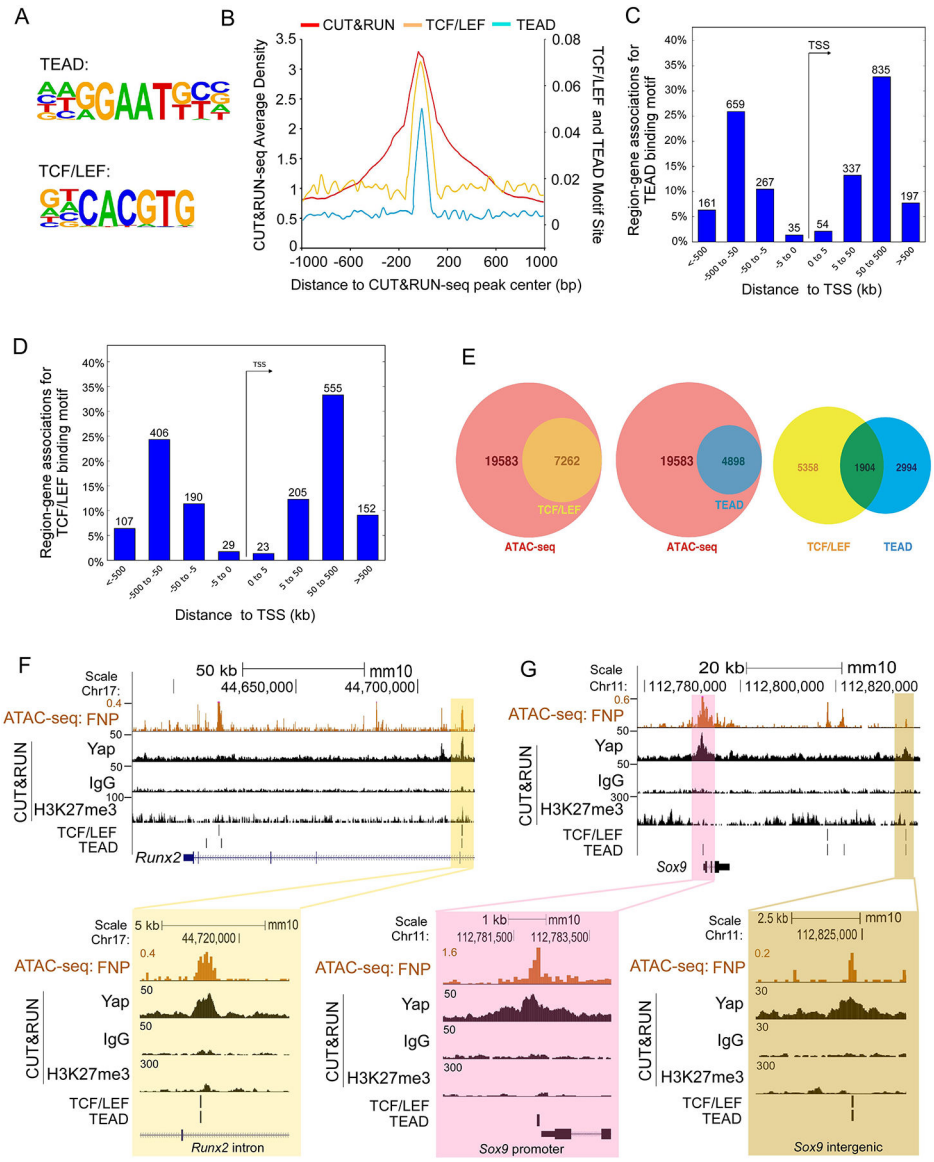

Fig 5. Yap and β-catenin coordinately regulate target gene expression in NCCs.

(**A and B**) TEAD and TCF/LEF motifs (A) and their enrichment in Yap CUT&RUN-seq data (B). The graph shows the distance between the average density of CUT&RUN-seq and average enrichment of TEAD and TCF/LEF binding motifs (right y-axis) ± 1 kb to the center of CUT&RUN-seq peaks. (**C** and **D**) Distribution of distance from the transcriptional start site (TSS) to all peaks in the TEAD binding motif (C) or TCF/LEF binding motif (D). (**E**) Venn diagram showing overlapping genes between regions of ATAC-seq peaks and regions containing TEAD and TCF/LEF binding motifs in human NCCs, based on data re-analysis of published human NCC ATAC-seq data (43). (**F** and **G**) Examples of regulatory regions in *Runx2* (F) and *Sox9* (G) genes in the alignment of ATAC-seq data from the frontonasal process (FNP) of E10.5 mouse embryos with the CUT&RUN-seq data.

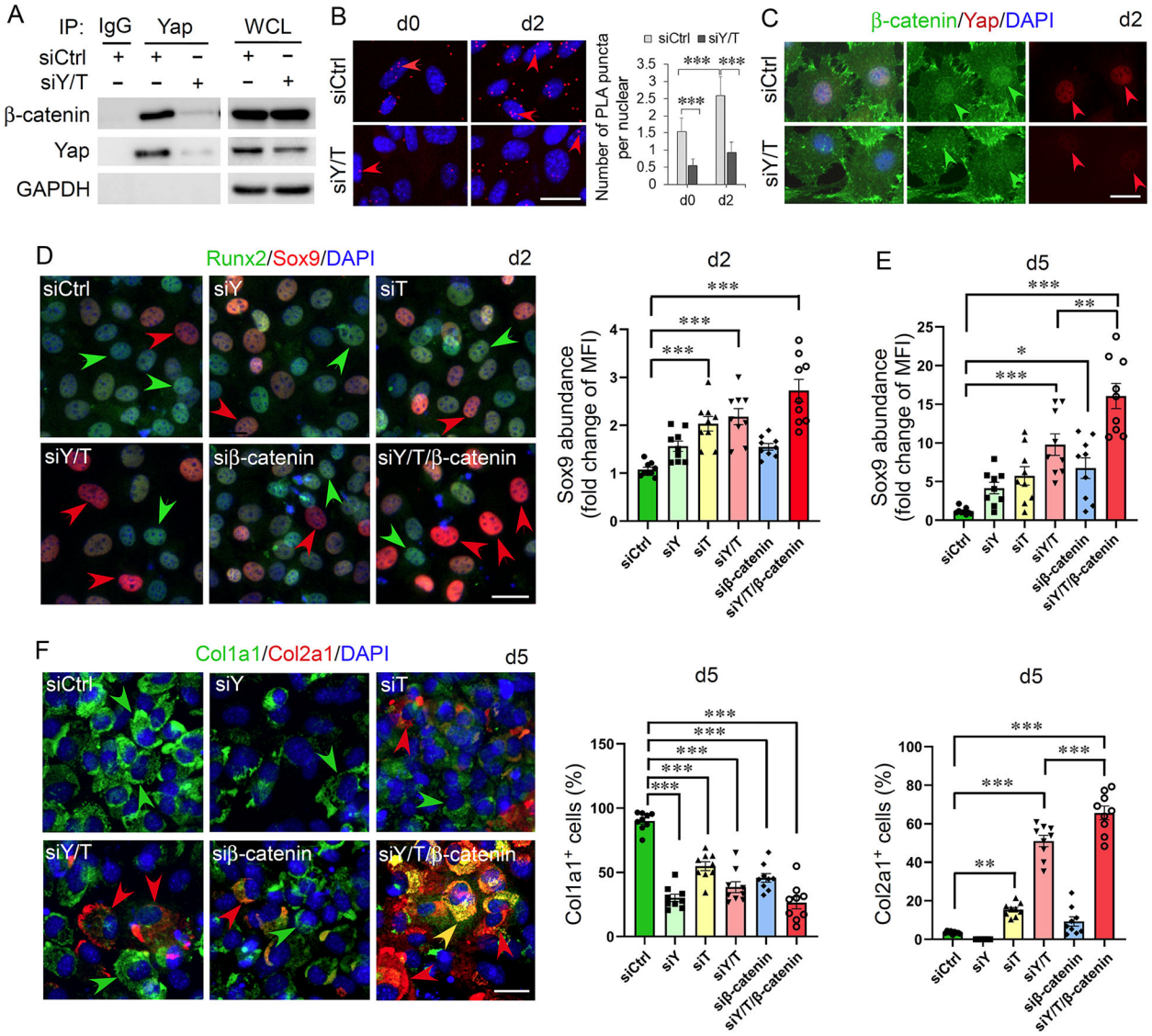

Fig 6. Yap and Taz cooperate with β-catenin to promote osteogenesis by preventing chondrogenesis in NCCs.

(**A**) Western blotting for β-catenin and Yap in Yap immunoprecipitates and whole cell lysates (WCL) of O9-1 NCCs treated with control siRNA (siCtrl) or siRNAs targeting *Yap* and *Taz* (siY/T). IgG immunoprecipitation is a negative control. GAPDH is a loading control. Data are representative of n = 4 independent experiments. (**B**) In situ proximity ligation assay (PLA) and quantification in siCtrl and siY/T O9-1 cells at d0 and d2 under osteogenic differentiation culture. Cells were counterstained with DAPI to label nuclei. The red arrowheads point to the interaction spots of Yap and β-catenin in the nuclei. Data are representative of n = 3 independent experiments. Scale bar, 25 μm. (**C**) Immunofluorescence staining for β-catenin and Yap in the nuclei of siCtrl and siY/T O9-1 cells at d2. The green and red arrowheads point to the nuclei enrichment of β-catenin and Yap, respectively. Data are representative of n = 3 independent experiments. Scale bar, 25 μm. (**D**) Representative images showing the osteogenic marker Runx2 and the chondrogenic marker Sox9 in control

(siCtrl), *Yap* KD (siY), *Taz* KD (siT), *Yap/TAZ* dKD (siY/T), *β-catenin* KD (siβ-catenin), and *Yap/Taz/β-catenin* triple KD (siY/T/β-catenin) O9-1 NCCs at d2 of culture under osteoblast differentiation conditions. The red and green arrowheads point to Sox9 and Runx2 cells, respectively. Sox9 abundance was quantified and compared among control and different KD cells. Data are representative of n = 3 independent experiments. Three different fields were analyzed in each independent experiment. MFI, mean fluorescence intensity. (**E**) Quantification results of Sox9 in control (siCtrl), *Yap* KD (siY), *Taz* KD (siT), *yAp/Taz* dKD (siY/T), *β-catenin* KD (siβ-catenin), and *Yap/Taz/β-catenin* triple KD (siY/T/β-catenin) O9-1 NCCs at d5 of culture under osteoblast differentiation conditions. Data are representative of n = 3 independent experiments. Three different fields were analyzed in each independent experiment. MFI, mean fluorescence intensity. (F) Representative images showing the osteogenic marker Col1a1 and the chondrogenic marker Col2a1 in the same cells as in (D) at d5 of culture under osteoblast differentiation conditions. The red and green arrowheads point to the $Col2a1^+$ and $Col1a1^+$ cells, respectively. Cells positive for each marker were quantified. Data are representative of n = 3 independent experiments. Three different fields were analyzed in each independent experiment. Scale bar, 25 μm. All quantitative data are shown as the mean ± SEM and are expressed as the fold-change relative to siCtrl for (D) and (E). For (B), the unpaired *t* test was used. For (D), (E) and (F), one-way ANOVA combined with Tukey's multiple comparisons test was used. $*p < 0.05$, $**p < 0.01$, $***p < 0.001$.

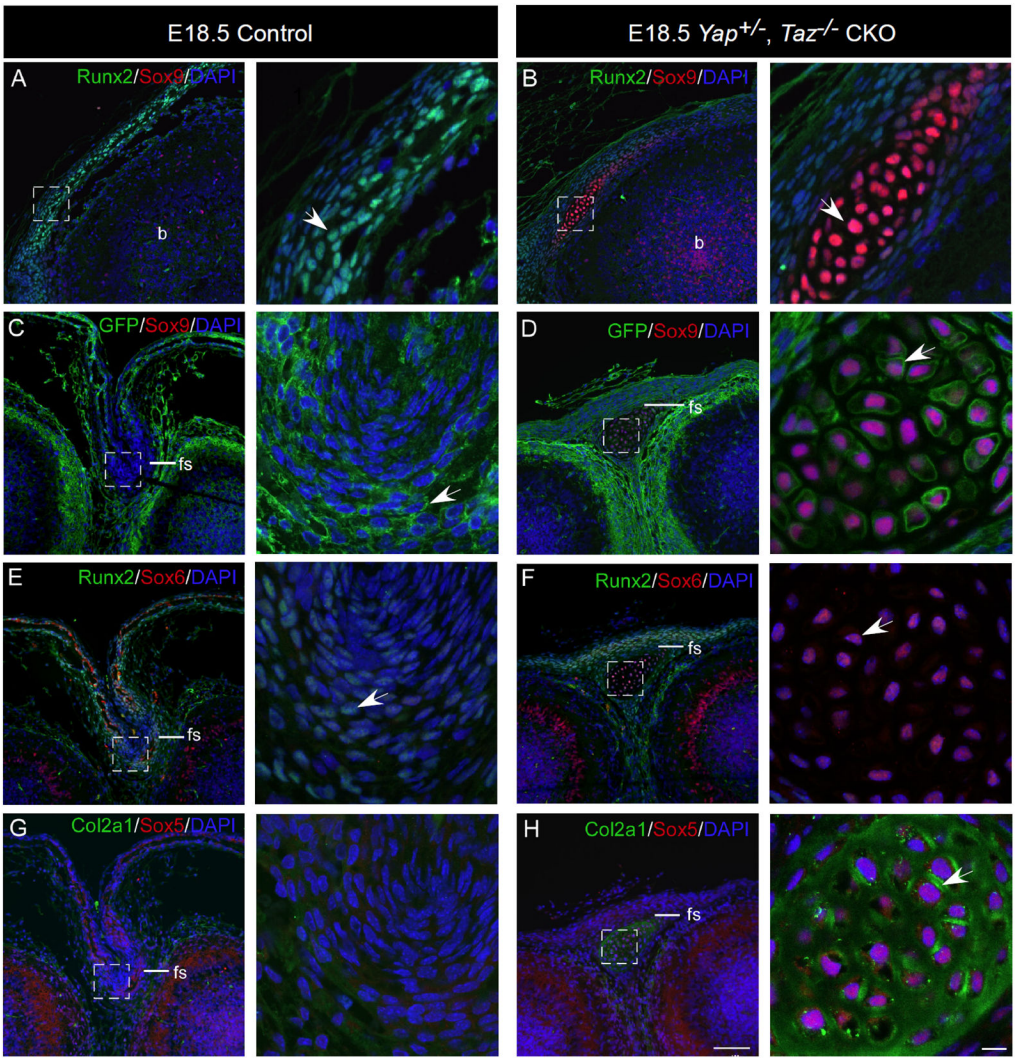

Fig 7. Yap and Taz regulate osteogenic and chondrogenic markers in vivo.

(**A** and **B**) Representative immunofluorescence IF (IF) staining for Runx2 and Sox9 in sagittal sections through the frontal bone of E18.5 *Wnt1-Cre2*$^{Tg/+}$;*Yap*$^{+/+}$;*Taz*$^{+/+}$ control (A) and *Yap*$^{+/−}$;*Taz*$^{−/−}$ CKO mutant embryos (B). Dashed boxes indicate the regions shown in the adjacent higher magnification images. The arrowheads indicate Runx2^{+} cells (A) and Sox9^{+} cells (B). (**C** and **D)** Representative IF staining for GFP, which labels all NCC-derived cells, and Sox9 in coronal sections through the frontal bone of E18.5 *Wnt1-Cre2*$^{Tg/+}$;*Yap*$^{+/+}$;*Taz*$^{+/+}$;*mTmG*$^{+/−}$ control (C) and *Yap*$^{+/−}$;*Taz*$^{−/−}$ CKO mutant embryos (D). The arrowheads indicate GFP^{+} cells (C) and GFP^{+}Sox9^{+} double-positive cells (D). (**E** and **F**) Representative IF staining for Runx2 and Sox6 in coronal sections through the frontal bone of E18.5 *Wnt1-Cre2* $^{Tg/+}$;*Yap*$^{+/+}$;*Taz*$^{+/+}$;*mTmG*$^{+/−}$ control (E) and *Yap*$^{+/−}$;*Taz*$^{−/−}$ CKO mutant (F) embryos. The arrowheads indicate Runx2^{+} cells (E) and Runx2^{+}Sox6^{+} double-positive cells (F). (**G** and **H**) Representative IF staining for Col2a1 and Sox5 in coronal sections through the frontal bone of E18.5 *Wnt1-Cre2* $^{Tg/+}$;*Yap*$^{+/+}$;*Taz*$^{+/+}$;*mTmG*$^{+/−}$ control (G) and *Yap*$^{+/−}$, *Taz*$^{−/−}$ CKO mutant embryos (H). The arrowheads indicate Col2a1^{+}Sox5^{+} double-positive cells. All scale bars, 100 μm (low magnification) and 10 μm (high

magnification). In all samples, nuclei were stained with DAPI (blue). All images are representative of at least 3 embryos per genotype. b, brain; fb, frontal bone; fs, frontal suture; nb, nasal bone.

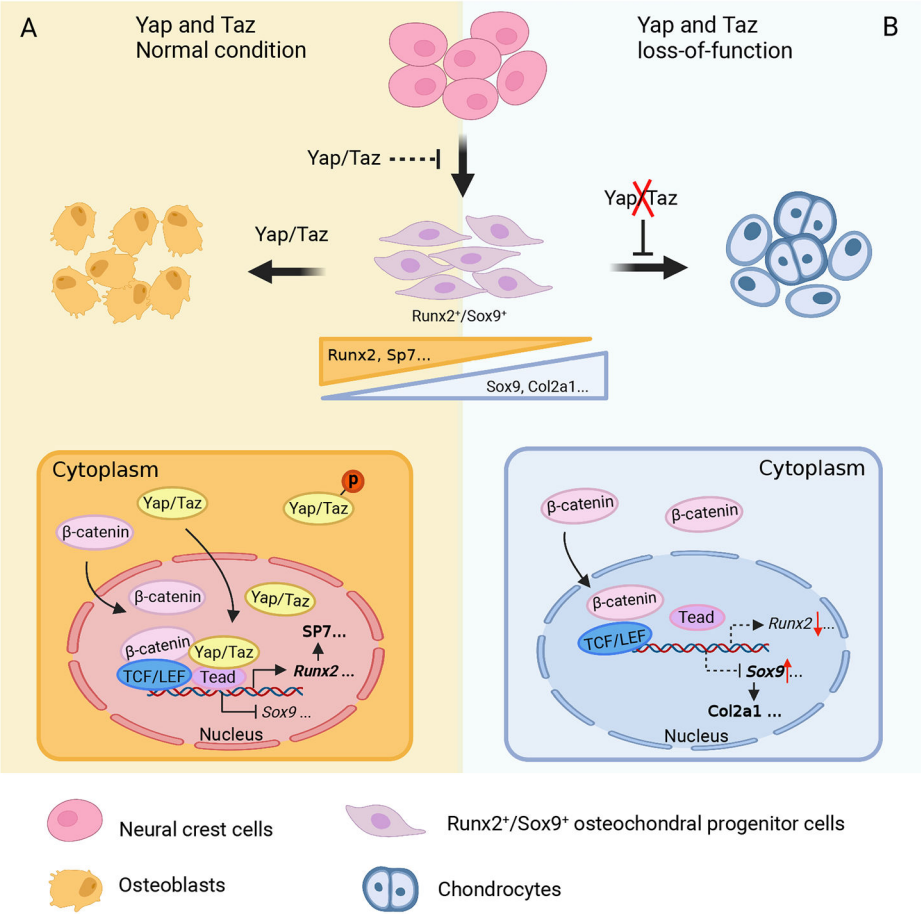

Fig 8. Working model for how Yap and Taz cooperate with β-catenin to promote osteogenesis and prevent chondrogenesis in NCCs.

(**A** and **B**) Yap and Taz likely maintain the stemness of NCCs and prevent them from differentiating. After NCCs are committed as $Runx2^{+}Sox9^{+}$ osteochondral progenitors, Yap and Taz promote osteogenesis and prevent chondrogenesis. In the NCC-derived osteochondral progenitors with normal expression of Yap and Taz (A), Yap/Taz/Tead could interact with β-catenin/TCF/LEF to promote osteogenesis by activating the expression of osteogenic genes such as *Runx2*, and prevent chondrogenesis by repressing the expression of chondrogenic genes such as *Sox9*. In the absence of Yap and Taz (B), osteochondral progenitors have decreased expression of osteogenic genes and increased expression of chondrogenic genes, leading to chondrogenesis instead of osteogenesis. This figure was created with BioRender.